ADAS applications for ITER

Robin Barnsley(1) and Martin O'Mullane, with ITER and EFDA/JET contributors

(1) Queen's University Belfast and EFDA/JET

Visiting researcher at ITER International Team, Garching, Germany

1) Confirming a measurement requirement
   Divertor VUV spectroscopy

2) Input to a diagnostic design
   X-ray crystal spectrometer

3) New measurement opportunities
   Spectroscopic x-ray camera

4) Input to machine design design
   Oxygen radiated power for input to leak spec.

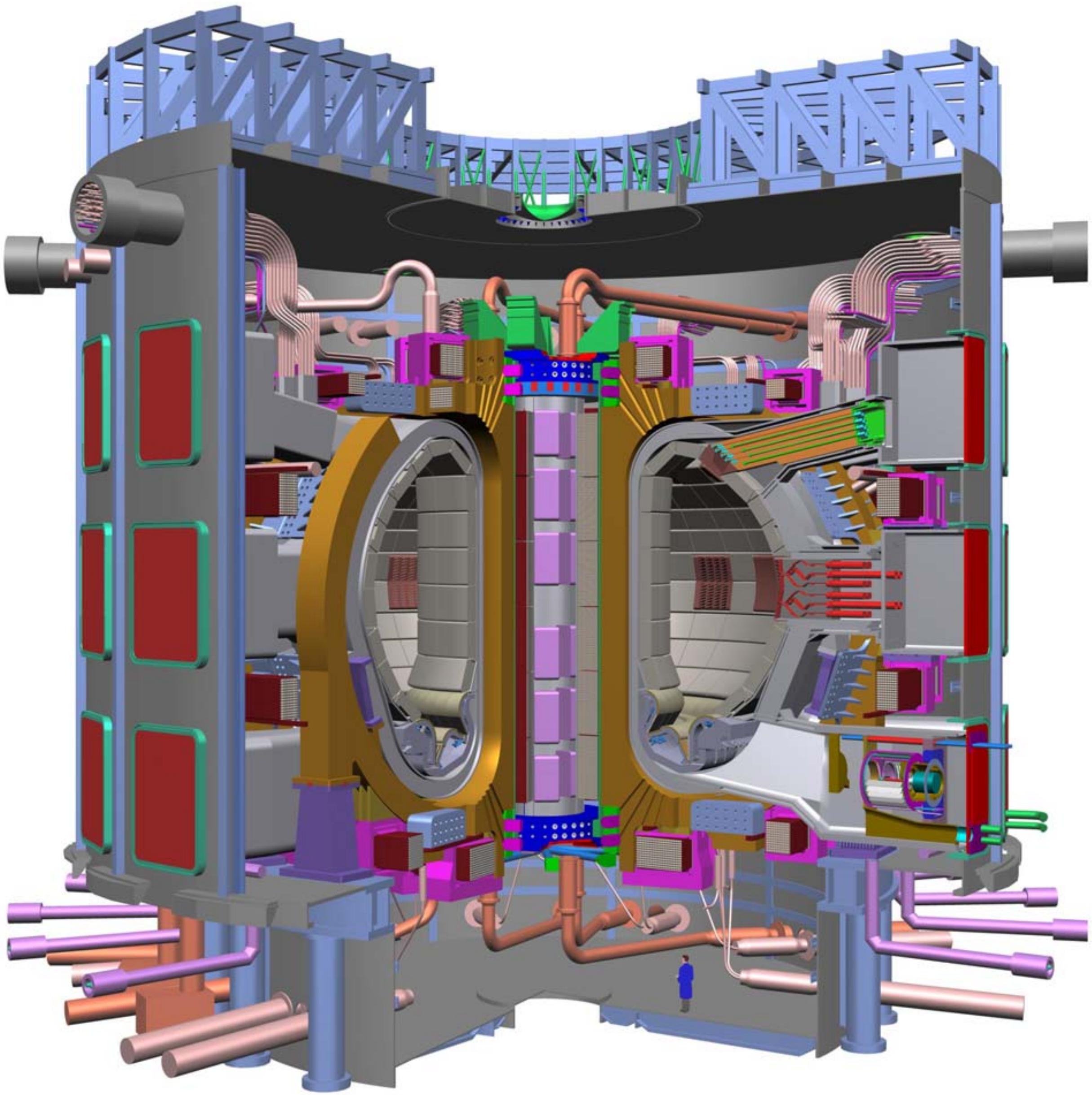

ITER (www.iter.org)

- Superconducting Tokamak
- Single-null divertor
- Elongated, triangular plasma
- Additional heating from RF, and negative-ion neutral-beams and

R (m)	6.2
a (m)	2
V_P (m^3)	850
I_P (MA)	15(17)
B_t (T)	5.3
δ,κ	1.85, 0.5
P_{aux} (MW)	40-90
P_α (MW)	80+
Q (P_{fus}/P_{in})	10
Pfus(MW)	500

ITER cross-section

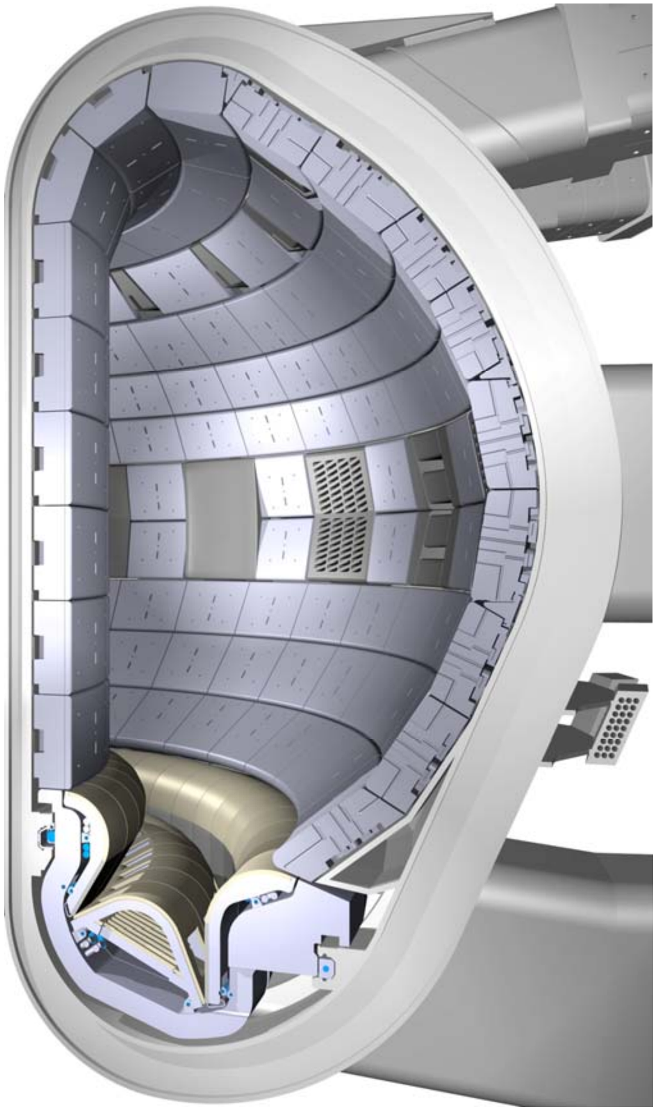

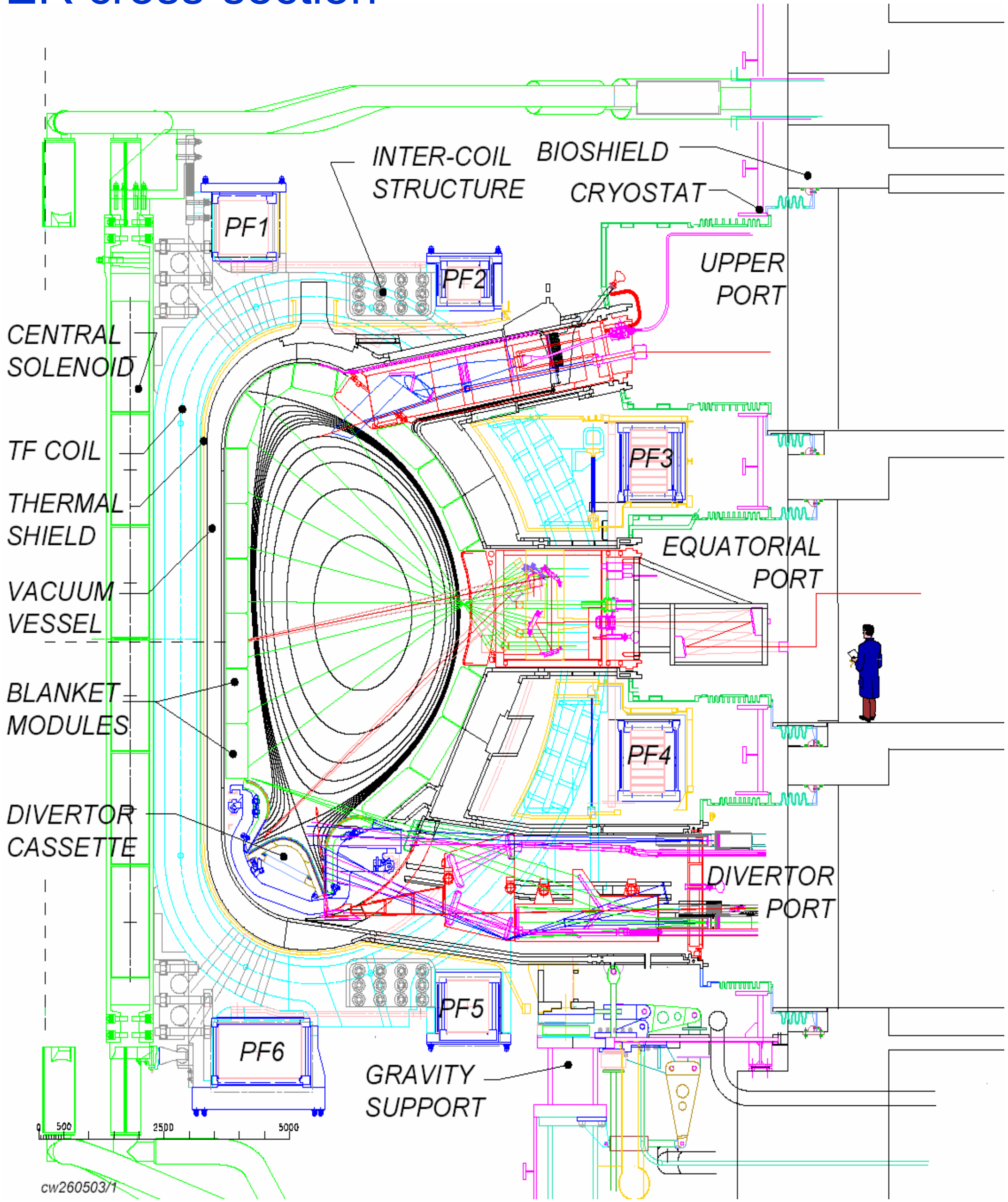

ITER Construction Schedule

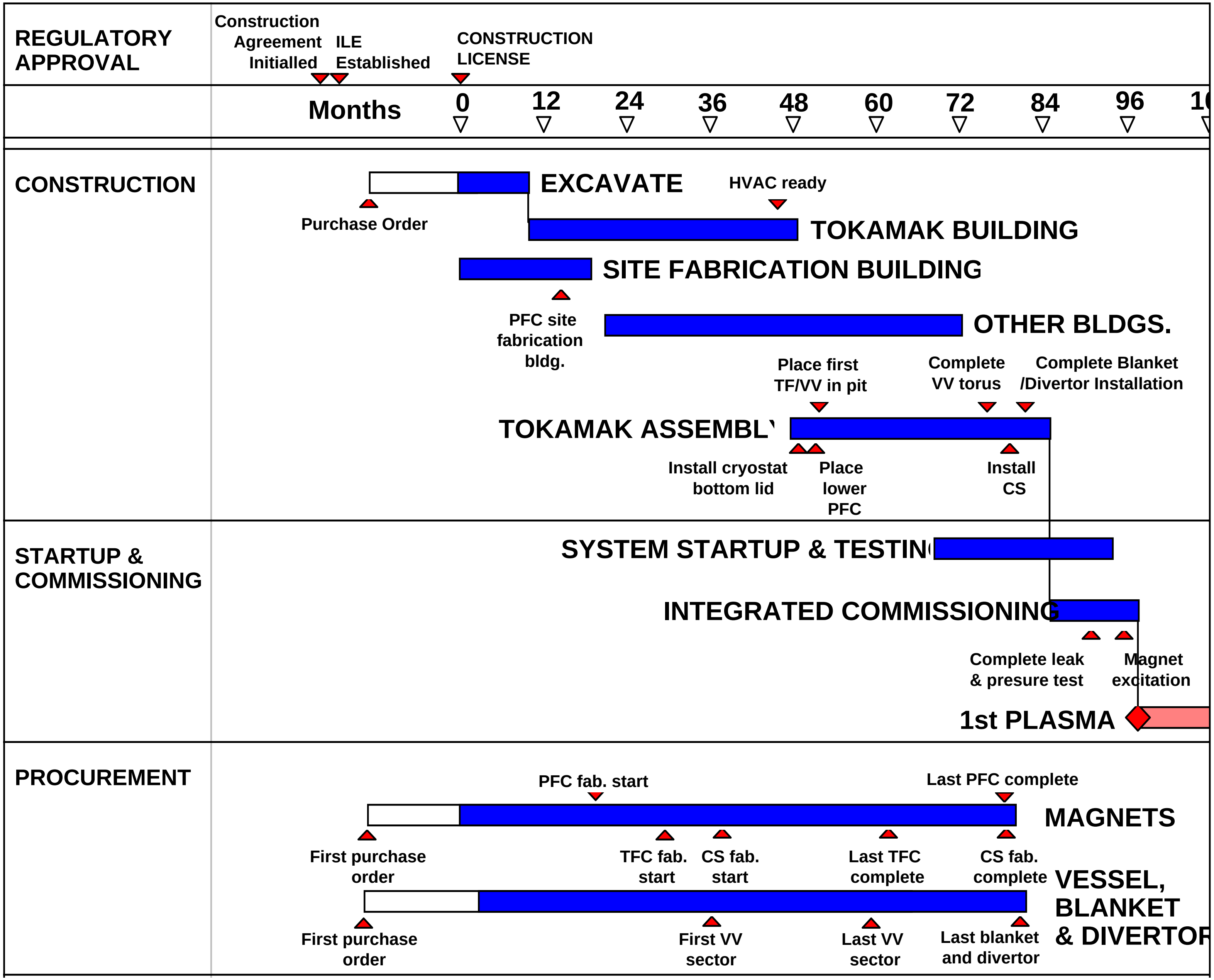

ITER Operation Schedule

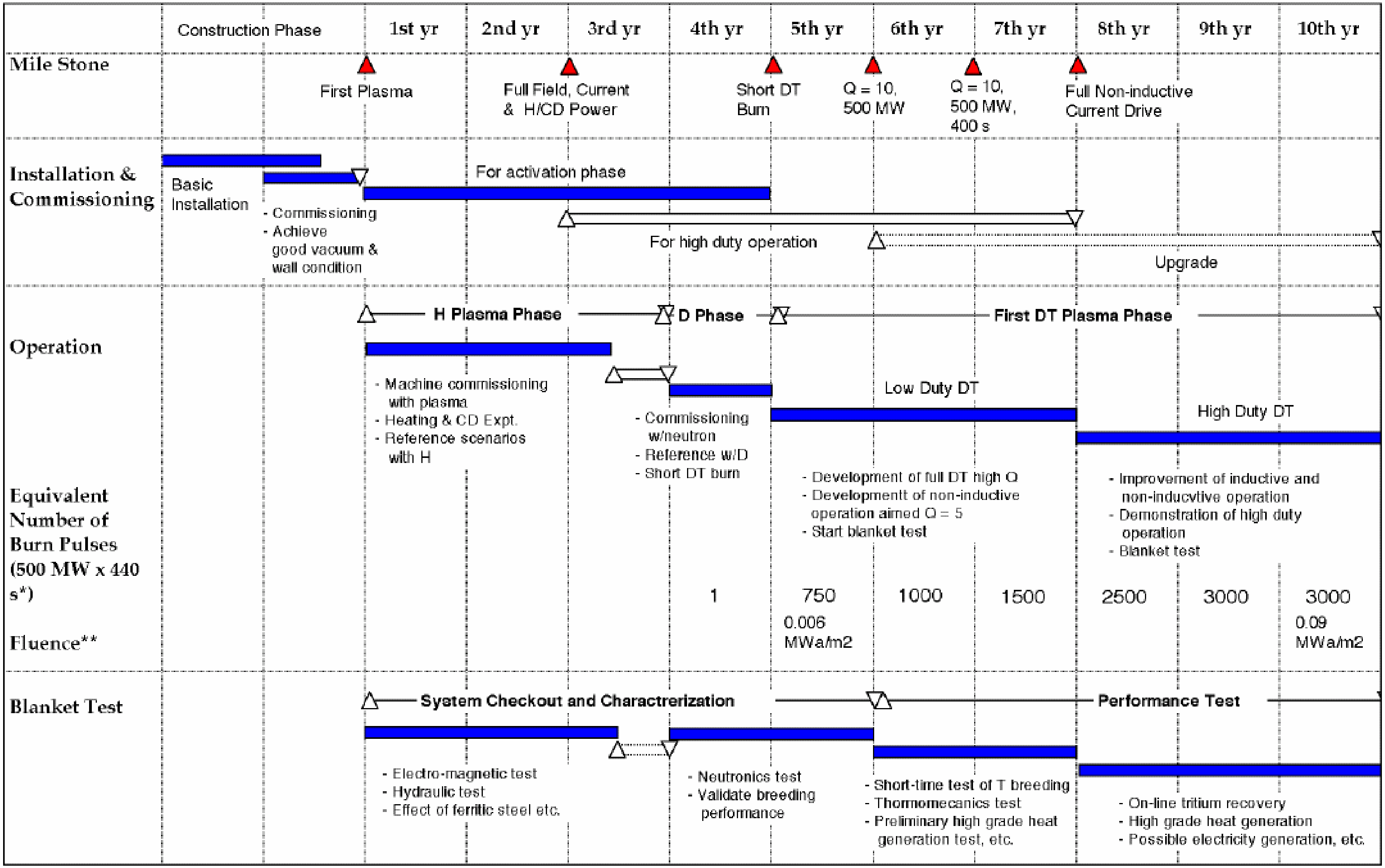

ITER Diagnostic Systems

Magnetic Diagnostics	**Spectroscopic and NPA Systems**
Vessel Magnetics	CXRS Active Spectr. (based on DNB)
In-Vessel Magnetics	H Alpha Spectroscopy
Divertor Coils	VUV Impurity Monitoring (Main Plasma)
Continuous Rogowski Coils	Visible & UV Impurity Monitoring (Div)
Diamagnetic Loop	X-Ray Crystal Spectrometers
Halo Current Sensors	Visible Continuum Array
Neutron Diagnostics	Soft X-Ray Array
Radial Neutron Camera	Neutral Particle Analysers
Vertical Neutron Camera	Laser Induced Fluorescence (N/C)
Microfission Chambers (In-Vessel) (N/C)	MSE based on heating beam
Neutron Flux Monitors (Ex-Vessel)	**Microwave Diagnostics**
Gamma-Ray Spectrometers	ECE Diagnostics for Main Plasma
Neutron Activation System	Reflectometers for Main Plasma
Lost Alpha Detectors (N/C)	Reflectometers for Plasma Position
Knock-on Tail Neutron Spectrom. (N/C)	Reflectometers for Divertor Plasma
Optical/IR Systems	Fast Wave Reflectometry (N/C)
Thomson Scattering (Core)	**Plasma-Facing Components and Operational Diagnostics**
Thomson Scattering (Edge)	IR Cameras, visible/IR TV
Thomson Scattering (X-Point)	Thermocouples
Thomson Scattering (Divertor)	Pressure Gauges
Toroidal Interferom./Polarimetric System	Residual Gas Analyzers
Polarimetric System (Pol. Field Meas)	IR Thermography Divertor
Collective Scattering System	Langmuir Probes
Bolometric System	**Diagnostic Neutral Beam**
Bolometric Array For Main Plasma	
Bolometric Array For Divertor	

- **Measurements for**:
- Machine protection
- Plasma control
- Physics studies
- ~45 parameters in total

ITER diagnostics are port-based where possible

Each diagnostic port-plug contains an integrated instrumentation package

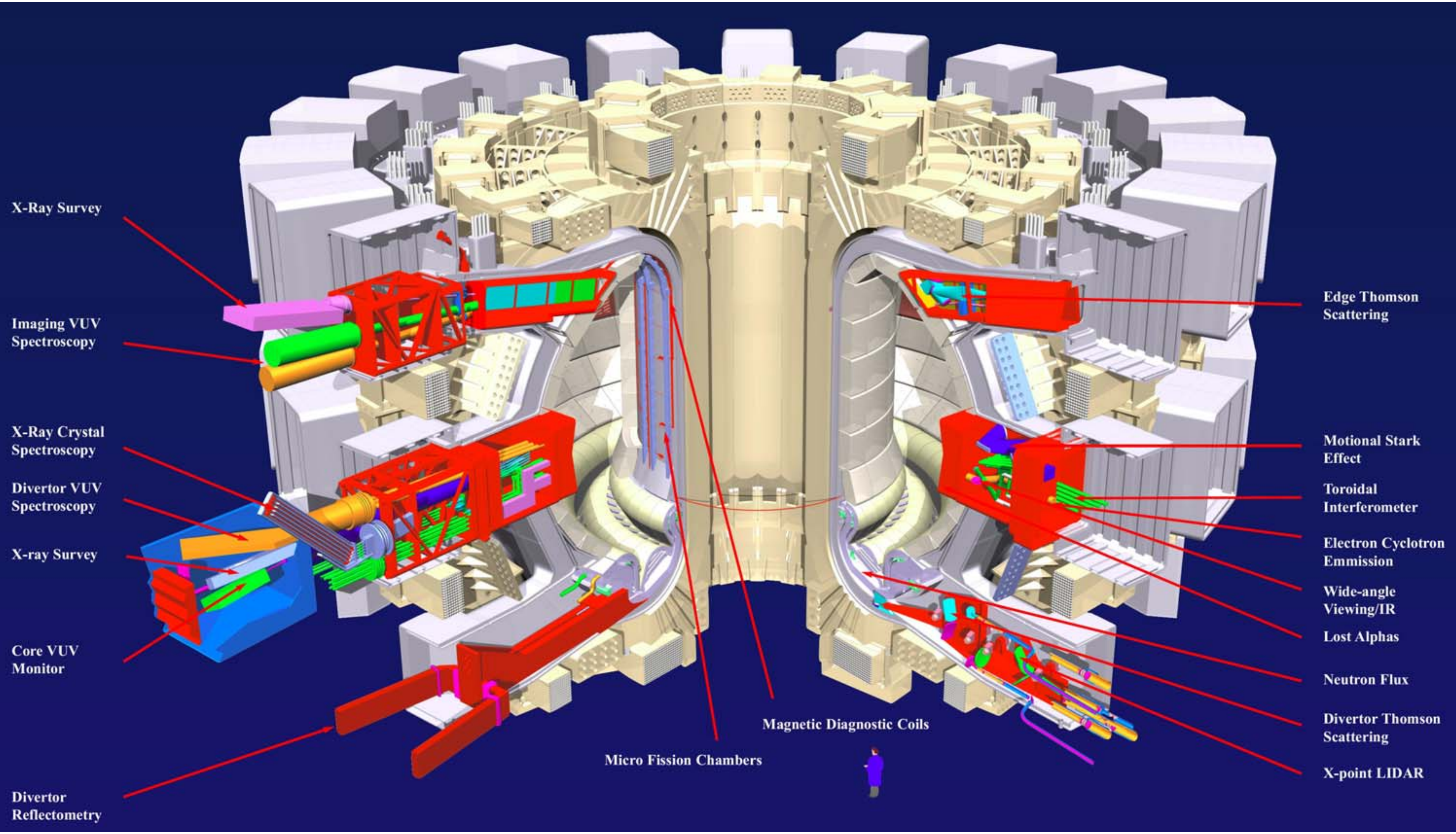

ITER diagnostic equatorial-port allocations

Each port has a lead diagnostic and lead Party

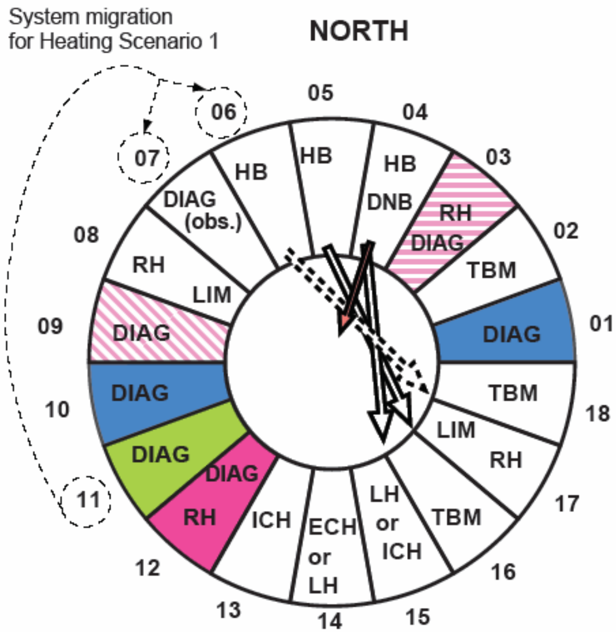

EQUATORIAL PORT

01
- **G01** Vis. / IR TV (1 of 4)
- **B01** Radial Neutron Camera
- **D01** Bolometry
- **E11** MSE (core, HB4)
- **E04** Divertor Impurity Monitor
- **B07** Gamma Ray Spectroscopy
- **B11** High Resolution Neutron Spectr
- **B09** Lost Alpha

03
- **G01** Vis. / IR TV (2 of 4)
- **E12** CXRS edge (on the DNB)
- **E11** MSE (edge, HB5)
- **E02** H-a Spectroscopy (divertor inner)

07
- **B08** Activation System (16N, 1 of 2)
- **B08** Activation System (foil, 1 of 2)
- **B04** Neutron Flux Monitor (DD)

08
- **B04** Neutron Flux Monitor (DT)

09
- **G01** Vis. / IR TV (3 of 4)
- **C05** Toroidal Interferometer/Polarimeter
- **E05** X-Ray Crystal Spect (Imaging)
- **F01** ECE,
- **F07** Fast Wave Reflectometry
- **E07** Soft X-ray Array

10
- **C01** Thomson Scattering main plasma)
- **C06** Polarimeter
- **C08** Thomson Scattering (inner divertor)

11
- **05** X-ray Crystal Spect (survey)
- **E03** VUV (main and divertor)
- **F02** Reflectometry LFS(main plasma)
- **E08** NPA
- **E04** Div Spectroscopy (VUV)

12
- **G01** Vis. / IR TV (4 of 4)
- **E02** H-a Spect (upper edge)
- **E06** Visible Continuum Array
- **C07** CT

17
- **B04** Neutron Flux Monitor (DT)
- **B08** Activation System (16N, 1 of 2)
- **B08** Activation System (foil, 2 of 2)

CN | EU | JA | KO | RF | US | FLEX | HOST | FUND

G55GR174-Alloc_col_2005-10-01.eps

ITER diagnostic upper-port allocations

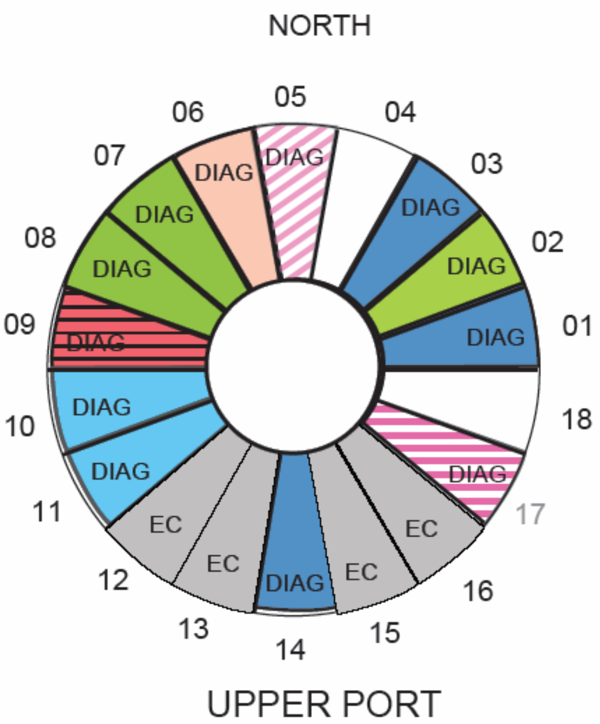

01 **F03** Position Reflectometry (1 of 2)
E04 Divertor Impurity Monitor
B08 Activation System (16N, 1 of 2)

02 **G10** Vis. / IR TV (1 of 6)
E02 Ha spectroscopy (divertor outer)
E02 Ha spectroscopy (outer edge)

03 **E01** CXRS core (on the DNB)

05 **G10** Vis. / IR TV (2 of 6)
B08 Activation System (16N, 2 of 2)

06 **E03** VUV grazing image (x 2)
B08 Activation System (foil, 1 of 2)

07 **E02** H-a spectroscopy (inner edge)
E02 H-a spectroscopy (upper edge)

08 **G10** Vis. / IR TV (3 of 6)
F09 Main Reflectometry (1 of 3)
D01 Bolometry

09 **E05** X-ray Crystal Spectr (imaging)
F09 Main Reflectometry
F11 Refractometry

10 **C06** Polarimeter

11 **G10** Vis. / IR TV (4 of 6)
C02 Edge Thomson Scattering
B08 Activation System (foil, 2 of 2)

12 **C07** CTS, (ECH)

14 **G10** Vis. / IR TV (5 of 6)
E05 X-ray Crystal Spectrometry (survey)
F03 Position Reflectometry (2 of 2)

17 **G10** Vis. / IR TV (6 of 6)
F02 Main Reflectometry (3 of 3)
E05 X-ray Crystal Spectrometry (graphite)
D01 Bolometry,
E07 Soft X-ray Array

Note: All port ducts also contain Ann + N01 Diagnostic Wiring

ITER measurement requirements relevant for x-ray VUV spectroscopy

10. Plasma Rotation	VTOR		1 – 200 km/s	10 ms	a/30	30 %
	VPOL		1 – 50 km/s	10 ms	a/30	30 %
12. Impurity Species Monitoring	Be, C rel. conc.		$1\bullet10^{-4} – 5\bullet10^{-2}$	10 ms	Integral	10 % (rel.)
	Be, C influx		$4\bullet10^{16} – 2\bullet10^{19}$ /s	10 ms	Integral	10 % (rel.)
	Cu rel. conc.		$1\bullet10^{-5} – 5\bullet10^{-3}$	10 ms	Integral	10 % (rel.)
	Cu influx		$4\bullet10^{15} – 2\bullet10^{18}$ /s	10 ms	Integral	10 % (rel.)
	W rel. conc.		$1\bullet10^{-6} – 5\bullet10^{-4}$	10 ms	Integral	10 % (rel.)
	W influx		$4\bullet10^{14} – 2\bullet10^{17}$ /s	10 ms	Integral	10 % (rel.)
	Extrinsic(Ne,Ar, Kr) rel. conc.		$1\bullet10^{-4} – 2\bullet10^{-2}$	10 ms	Integral	10 % (rel.)
	Extrinsic (Ne, Ar, Kr) influx		$4\bullet10^{16} – 8\bullet10^{18}$ /s	10 ms	Integral	10 % (rel.)
23. Electron Temperature Profile	Core T_e	r/a < 0.9	0.5 – 40 keV	10 ms	a/30	10 %
	Edge T_e	r/a > 0.9	0.05 – 10 keV	10 ms	5 mm	10 %
28. Ion Temperature Profile	Core T_i	r/a < 0.9	0.5 – 40 keV	100 ms	a/10	10 %
	Edge T_i	r/a > 0.9	0.05 – 10 keV	100 ms	TBD	10 %
32. Impurity Density Profile	Fractional content, Z<=10	r/a < 0.9	0.5 – 20 %	100 ms	a/10	20 %
		r/a > 0.9	0.5 – 20 %	100 ms	50 mm	20 %
	Fractional content, Z>10	r/a < 0.9	0.01 – 0.3 %	100 ms	a/10	20 %
		r/a > 0.9	0.01 – 0.3 %	100 ms	50 mm	20 %

Spectral distribution of collection optics on ITER

Wavelength	System	1^{st} Mirr. or slots	Party	ADAS input
IR	Thermography	1		
IR-Vis-UV	Vis IR upper	6	**US**	
	Vis-IR, equatorial	4	**EU**	
	H-alpha	6	**RF**	
	Visible cont. array	1	**CN**	
	Divertor visible	3	**JA**	EU study
	Edge CXRS	2	**RF**	
	Core CXRS	1	**EU**	EU M.Von Hellerman
	MSE edge + core	2	**US**	
	TS (LIDAR, edgeTS, etc)	3	**EU JA RF**	Background light
VUV	Main plasma VUV	2	**KO**	EU STRAHL, W.Biel
	Divertor VUV	2		EU study
X-ray	X-ray survey spectrometer	1	**IN?**	O'Mullane 1997 Varenna
	High resolution x-ray	3	**US?**	EU studies 20034-6
	X-ray camera	1		ADAS/SANCO M.O'Mullane 2006
γ-ray	γ-ray spectrometer/camera	1		

Modelled Tungsten spectrum in ITER divertor

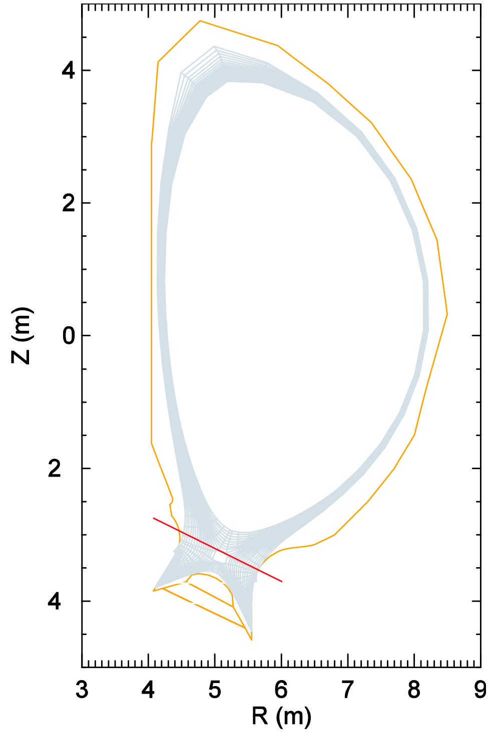

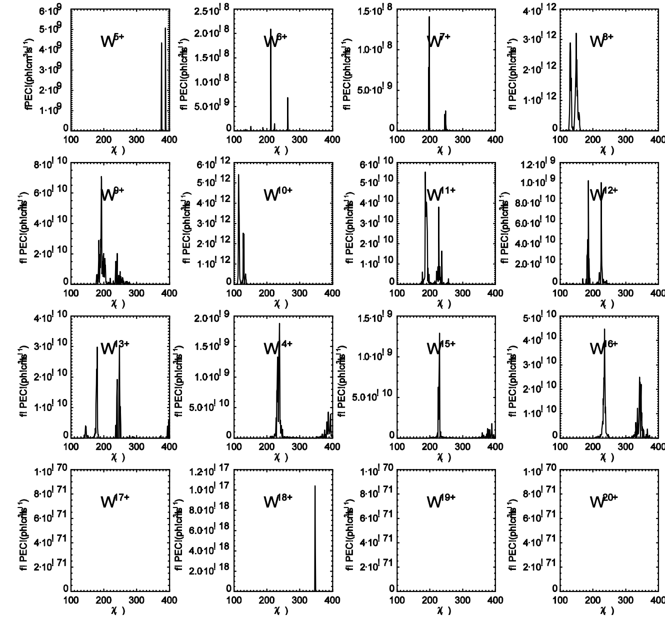

Left Modelled divertor sight-line

Right Spectra of individual W ionization stages

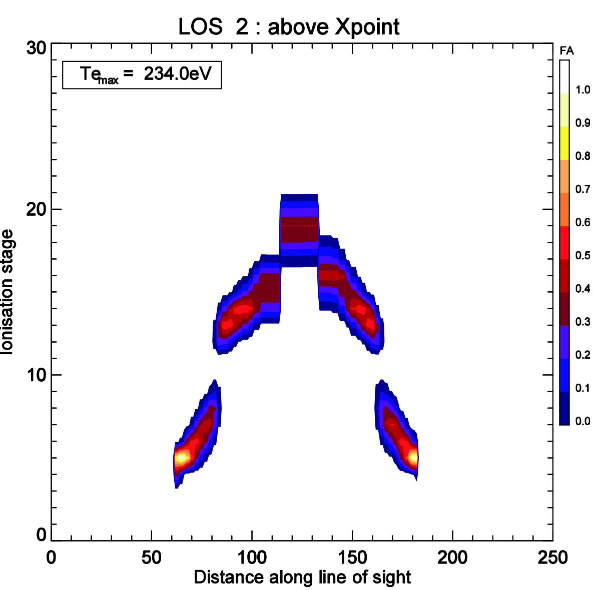

Left W ionization balance along divertor sight-line

Right Composite **W** spectrum

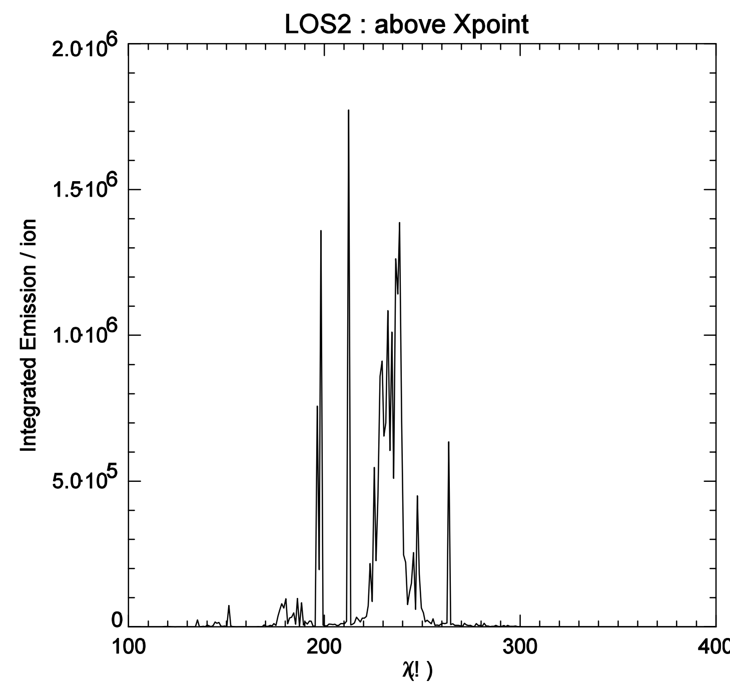

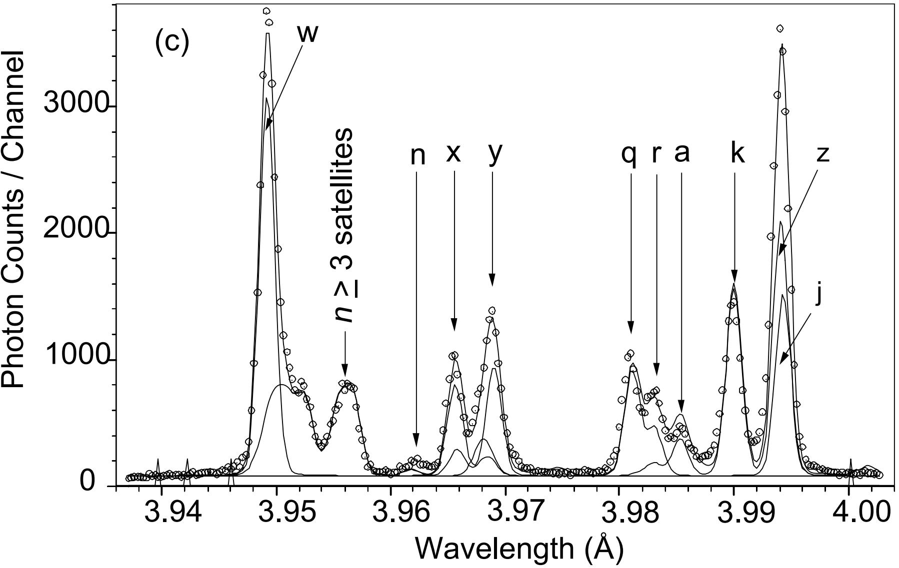

Te = 0.58 keV from <u>all</u> diel. satellites & line **w**; Ti = 0.45 keV

ArXVII spectrum from NSTX - Manfred Bitter

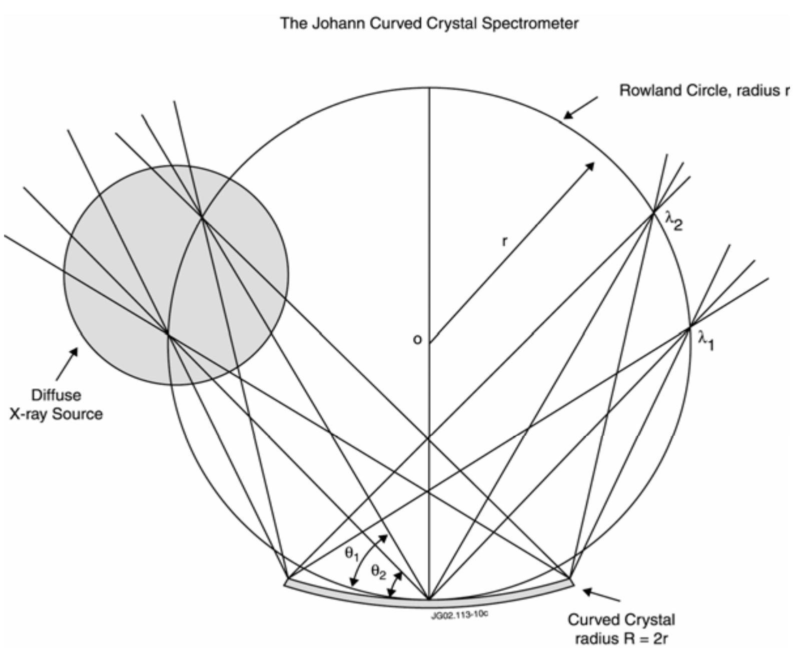

Credo in high-resolution x-ray spectroscopy

Extensively, but not exclusively, He-like ions.

~Te/Z: 250eV: Ne, 500eV,:Ar, 2keV: Fe-Ni, 10keV:Kr

Requires $\lambda/\delta\lambda$ >~ 5000, hence λ < 1.3 nm for crystals

Ti:	Doppler broadening
Vtor/pol:	Doppler shift
Te	Dielectronic satellite ratio
ne	Forbidden line ratio z/(x+y) (sometimes)
Zeff	Continuum τimp Impurity injection
nimp	Absolute calibration

Simple and reliable - bent crystal & pos. sens. detector.

Crystals are cheap dispersive elements, eg Si < 1kEur

Energy resolving detector makes it doubly dispersive, with excellent signal-to-noise ratio.

All crystal-window-detector processes are volume effects, leading to calculable and stable calibration. (1 mm Carbon ~ transparent at 10 keV).

Detector developments have been the key to progress:

1st gen.	Photographic film
2nd gen.	Multiwire prop. counter, ~ 3 - 25 m radiius
3rd gen.	Solid state eg CCD, 0.5 - 2 m radius
4th gen.	Imaging with fast 2-d detector

Doubly-curved crystal optics

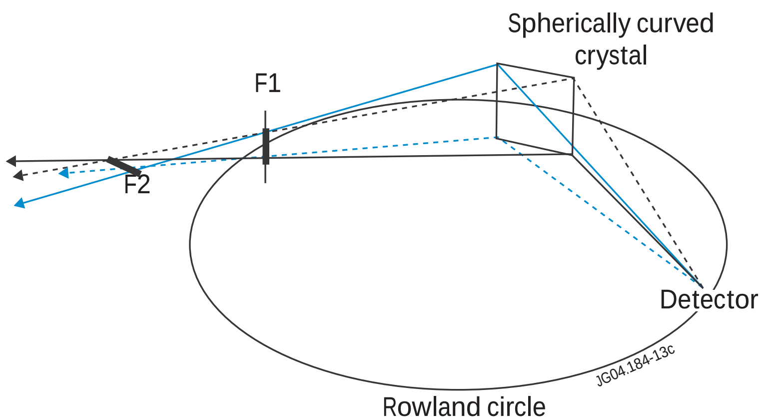

Fig.14a. Spherical crystal optics

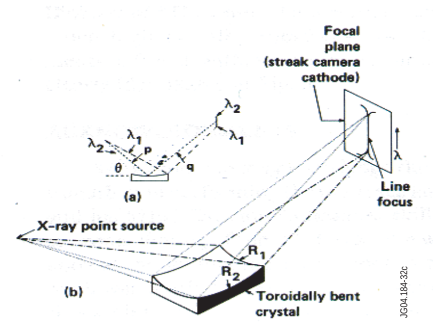

Fig.14b. Toroidal crystal optics

+ Spherical or toroidal crystal allows plasma imaging

+ Improves S/N ratio with smaller entrance aperture and smaller detector

$f_s/f_m = -1/\cos(2\theta_B)$

- No real focus for $\theta_B < 45°$

f_s: Sagittal focus f_m: Meridional focus θ_B: Bragg angle

2-D spectrum of He-like argon in TEXTOR. *G Bertschinger*

Left uncorrected spectrum. **Right** corrected for curvature of lines

Vignetting due to the input flange on TEXTOR.

The observation range is about 20% of the plasma, i.e. 9cm from a minor plasma radius of 45 cm.

Derived data from imaging crystal spectrometer on TEXTOR

G Bertschinger

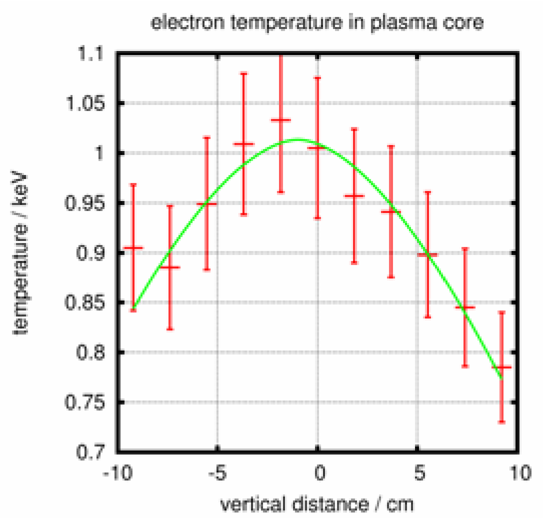

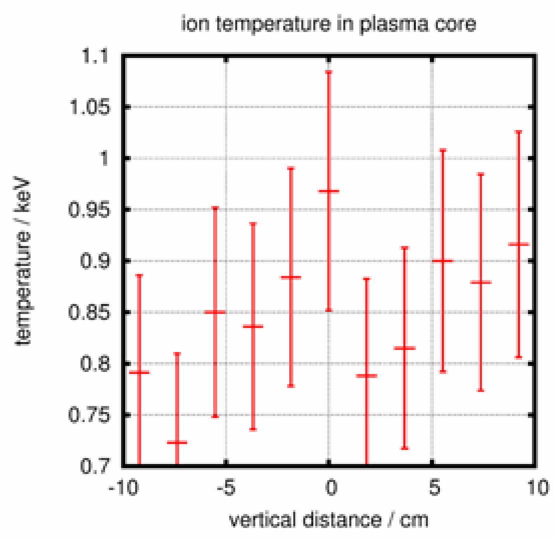

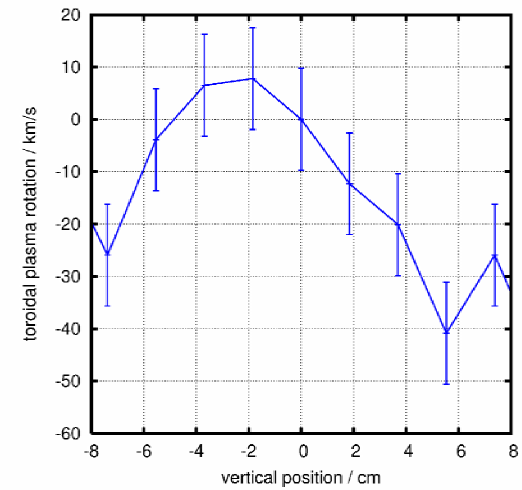

The electron temperature shows a clear dependence on the plasma radius.

No clear variation is detected for the ion temperature, within the errors of the measurement.

This is due to two reasons: I

1) In ohmic discharges, the ion temperature is broader than the electron temperature and therefore less variation over the limited observation range is expected.

2) The ion temperature is proportional to the square of the line width, whereas the electron temperature depends on the square root of the line ratio between the resonance line and the dielectronic satellite and therefore the errors are larger for the ion temperature.

The indicated variation of the plasma rotation over the radius is unrealistically large. In plasmas with ohmic heating, the total plasma rotation in the center is in the order of 25 km/s and decreases to the plasma edge.

The deviations are probably due to errors in the correction for the curved spectral lines, or non-linearities in the detector. For TEXTOR, these deviations can be measured and corrected by reversing the toroidal field and the plasma current.

High resolution imaging crystal spectrometer for ITER

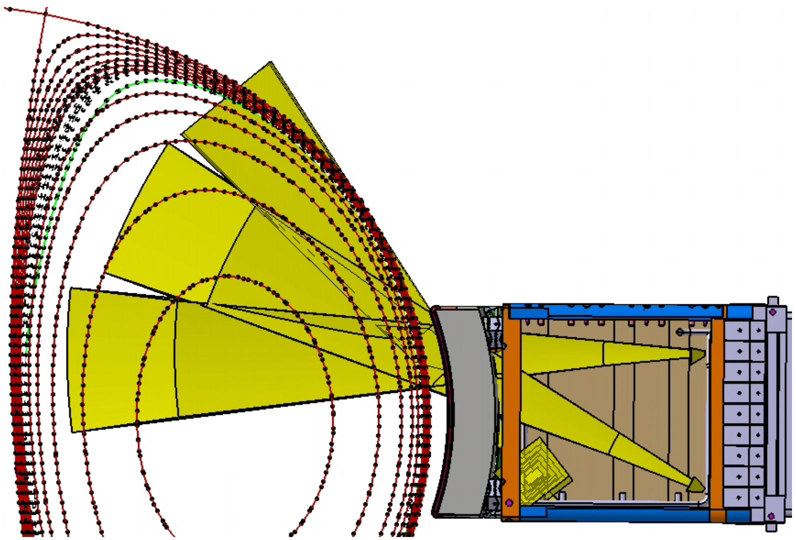

Plasma coverage by radial views

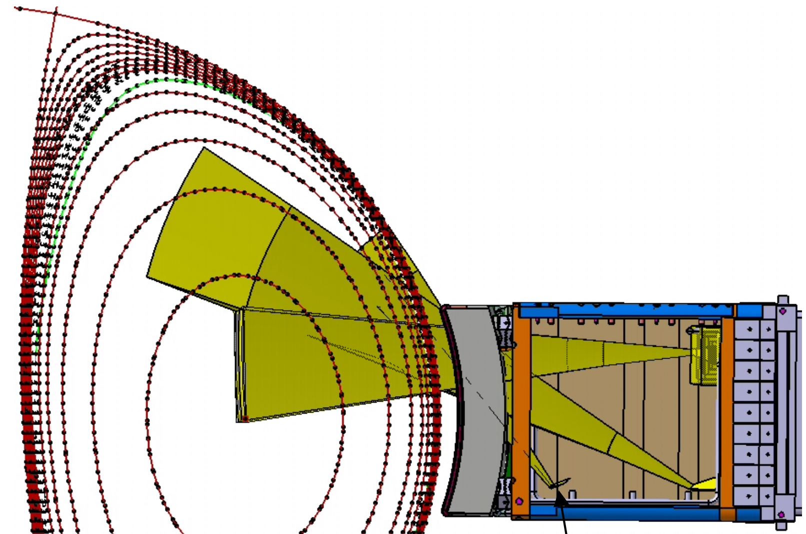

Plasma coverage by toroidal views

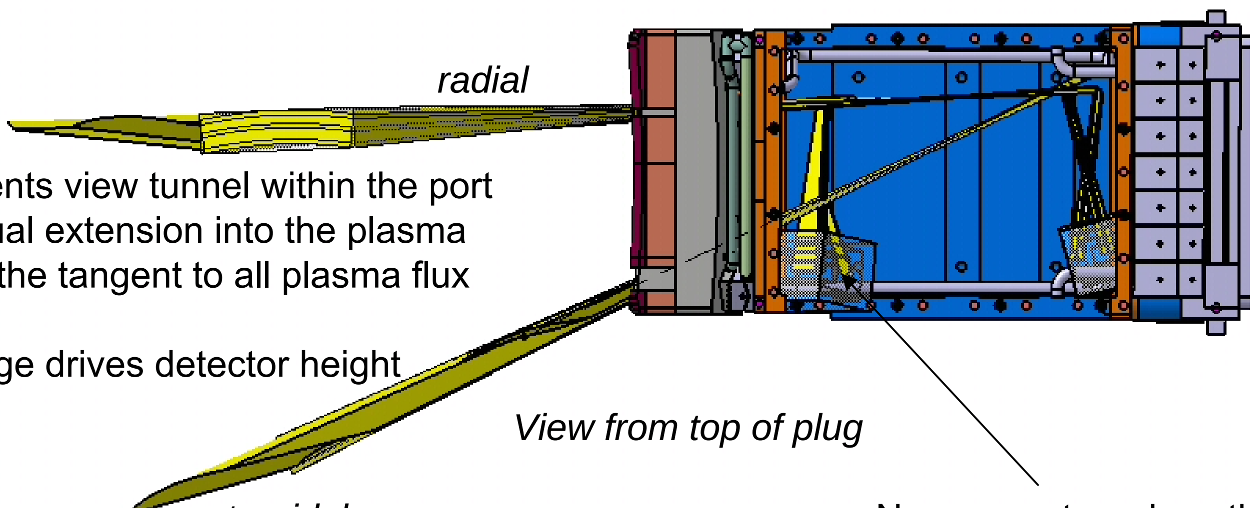

View from top of plug

- Yellow represents view tunnel within the port plug and its virtual extension into the plasma
- Aim is to view the tangent to all plasma flux surfaces
- Spatial coverage drives detector height

Necessary to reduce the crystal-detector distance for the furthest-forward toroidal view spectrometer

ITER radial profiles used for ADAS-SANCO and signal simulations.

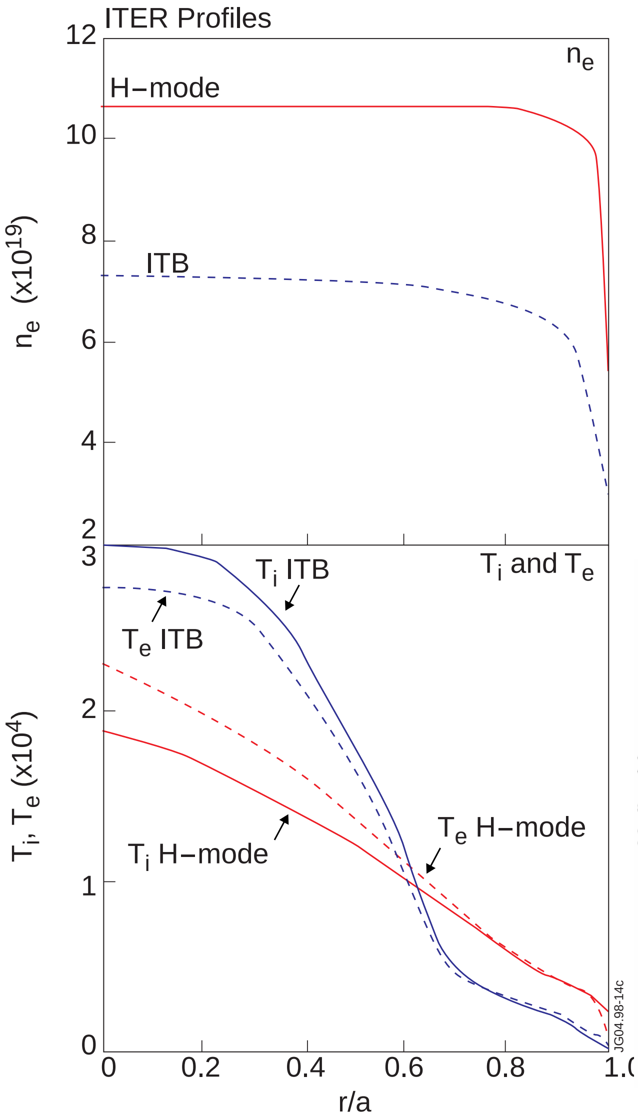

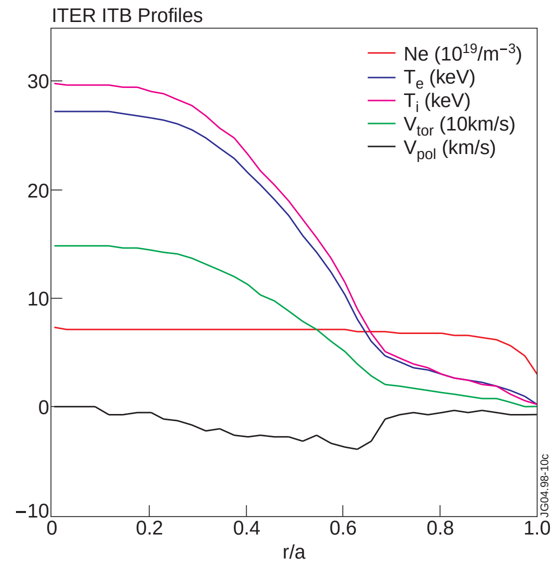

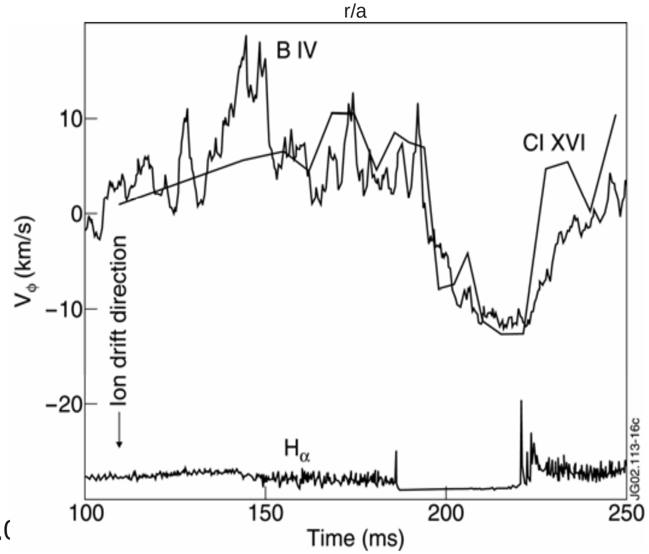

The most challenging Doppler measurement is the poloidal rotatiion

Toroidal rotation derived from centroid shifts of core Cl XVI lines in COMPASS-D.
V_{tor} of 2 km/s was measurable in ~10 ms

Table 5. Concentrations of Ar, Fe and Kr, for ΔP_{rad} = 500 kW in H-mode. The right-hand column gives a guide to efficiency of the impurity as a diagnostic tracer, in terms of count-rate per MW of ΔP_{rad}.

Ion	Wavelength (nm)	n_{imp} / n_e for ΔP_{rad} = 500kW	Count-rate for ΔP_{rad} = 500kW (MHz)	Count/ΔP_{rad} (MHz/MW)
Ar^{16+}	0.3948	$2 . 10^{-5}$	36	288
Ar^{17+}	0.3731		33	264
Fe^{24+}	0.1850	$6 . 10^{-5}$	17	42
Fe^{25+}	0.1778		16	40
Kr^{34+}	0.0946	$3.6 . 10^{-5}$	1.2	1.72
Kr^{35+}	0.0918		0.28	0.4

Incremental radiated power for added impurities

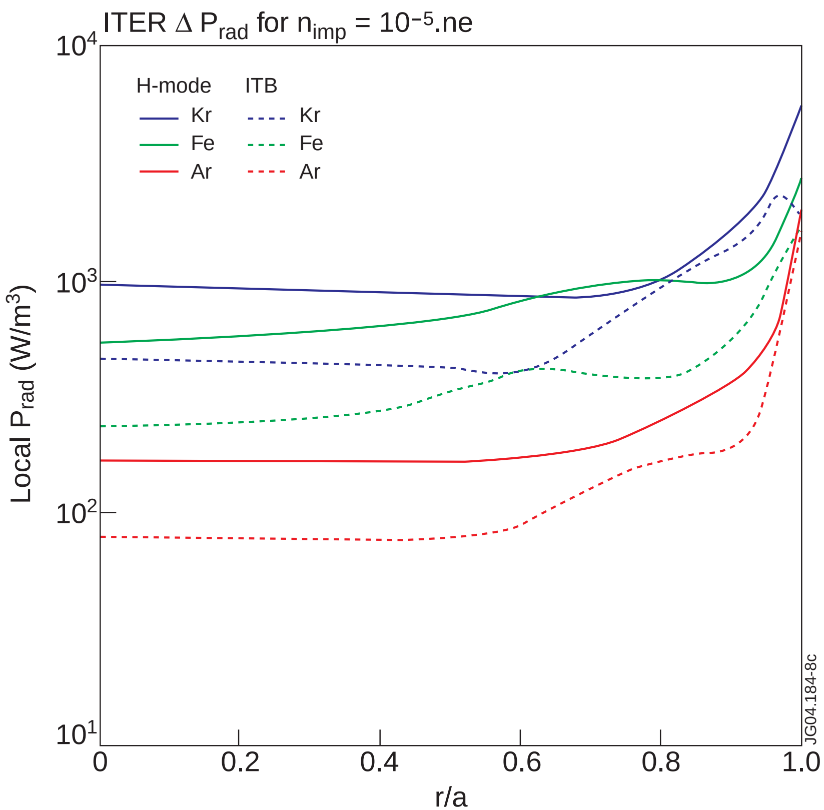

Radial profiles of local ΔP_{rad} for Ar, Kr & Xe
For H-mode and ITB plasmas, at $n_{imp}/n_e = 10^{-5}$.

The main constraint on the allowable added impurity concentration is not the increase in Z_{eff}, which is very small, but the additional radiated power, ΔP_{rad}.

The H-mode incremental radiated powers for added impurity concentrations of $10^{-5}.n_e$ are:

Ar 0.25 MW

Fe 0.8 MW

Kr 1.4 MW

ITB values are about 30% lower

All signal estimates are normalized to ΔP_{rad}. = 500 kW

Modelled emissivity and line/continuum ratios for ITB with $n_{imp}/n_e = 10^{-5}$.

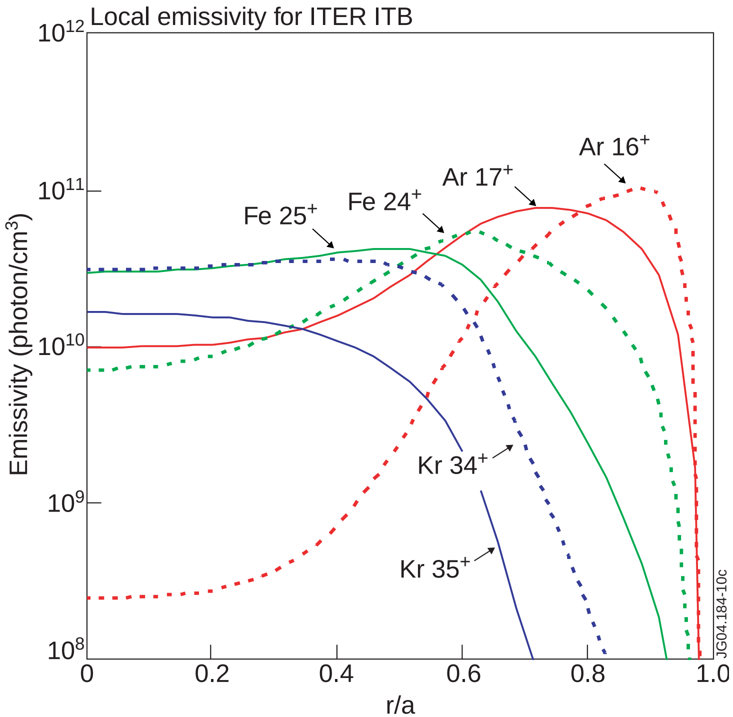

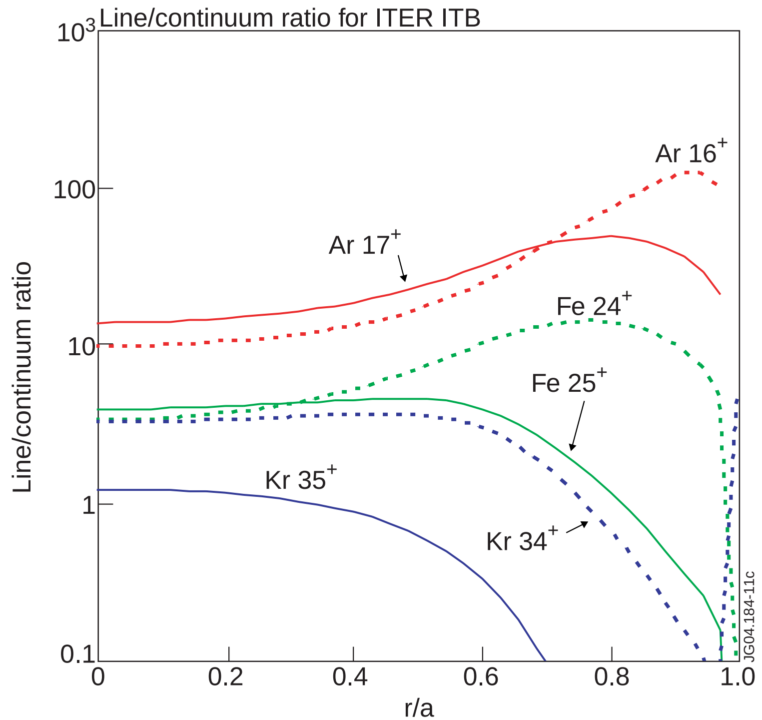

Left: Local photon emissivity

Right: Line/continuum ratios

ADAS-SANCO modelling for $n_{imp}/n_e = 10^{-5}$.

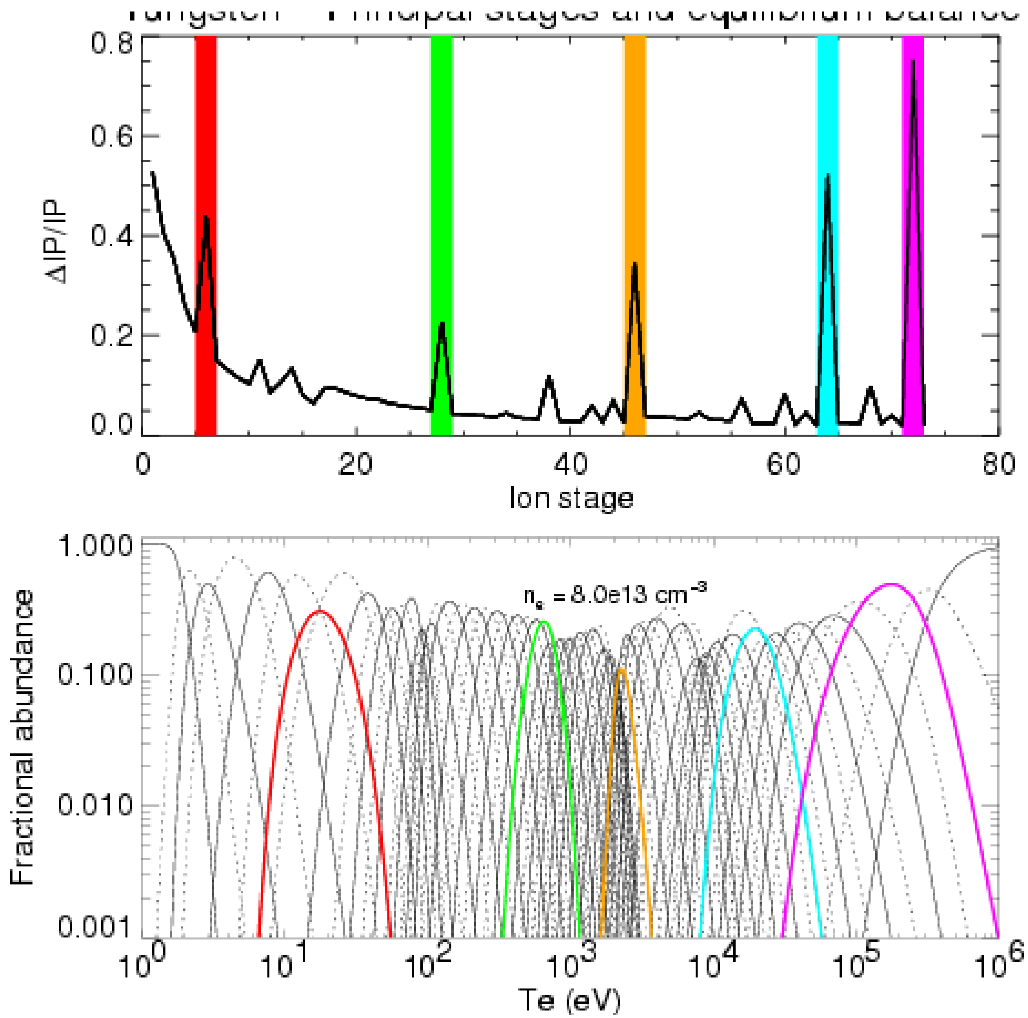

Fig.9. Coronal fractional abundance of W ions (below), with (above) a guide to the shells with greatest ionization potential ranges ΔIP/IP.

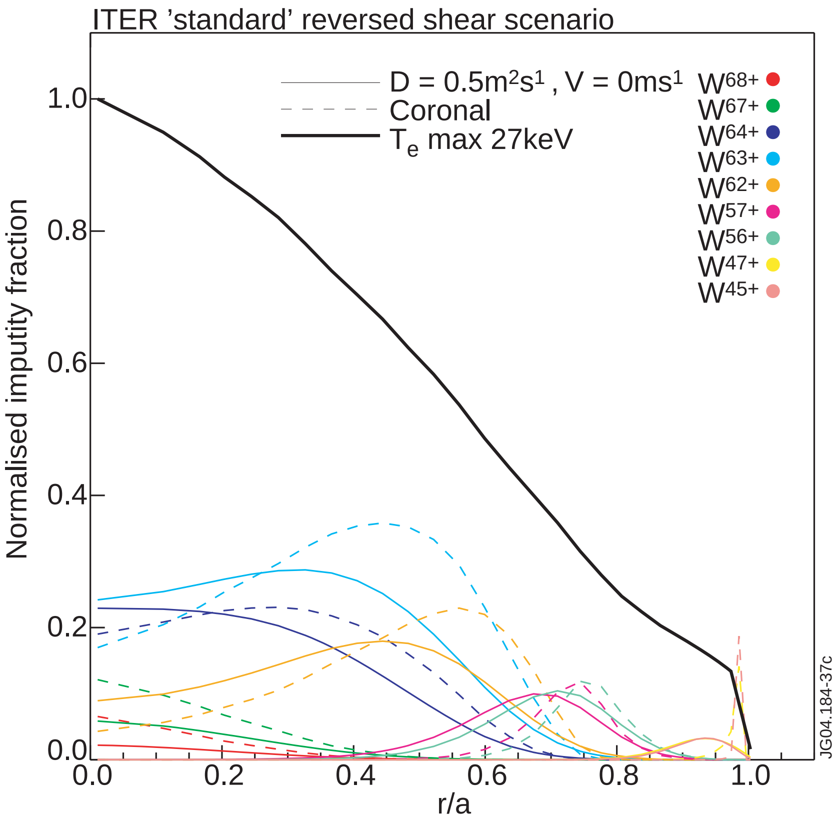

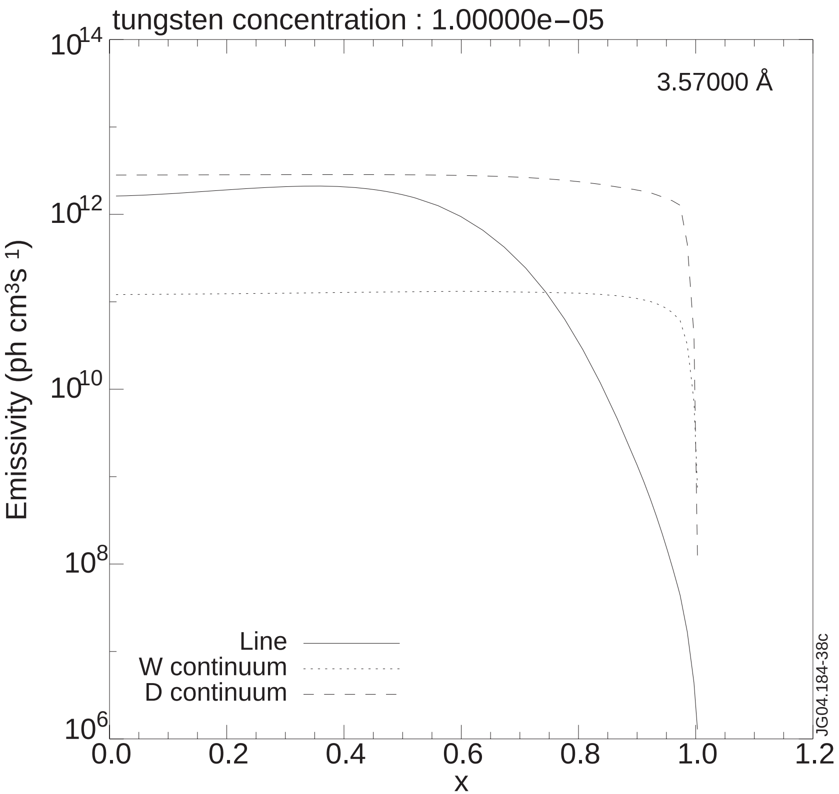

a. Fractional abundance for W ions.

b. W^{63+} emissivity.

Fig.10. SANCO-modelled ITB plasma with Tungsten, for $n_W=10^{-5}.n_e$

Modelled signals and detector requirements

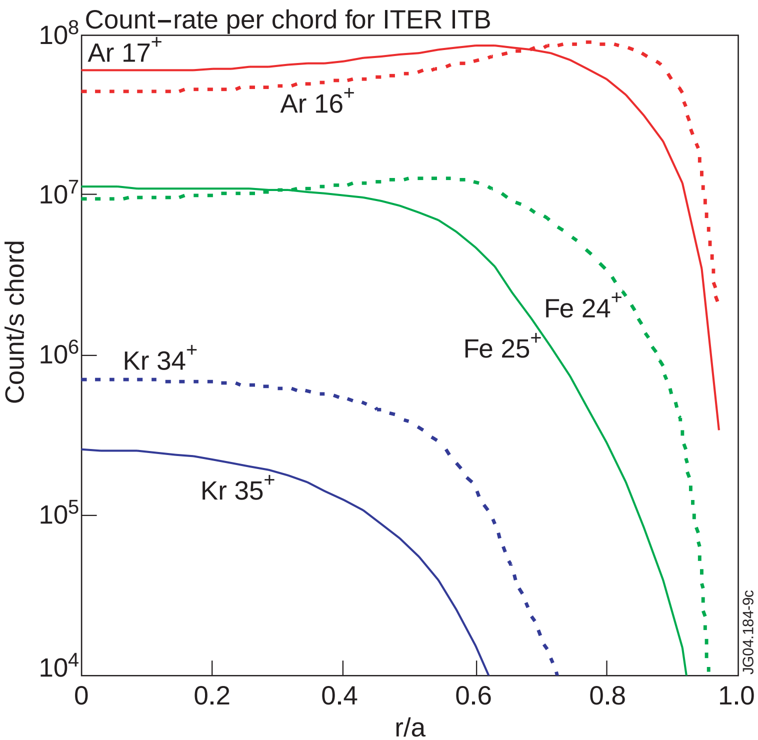

Simulated count-rates per chord for x-ray crystal spectrometer with 35 effective chords

These are line-of-sight integrals, because plasma is optically thin

Outline detector specification

Number of detectors	~ 6
Radiation hard	
Photon counting with at least one energy window	
Height (spatial)	~100 mm
Width (wavelength	~ 25 mm
Height resolution	~ 1 mm
Width resolution	~ 100 um
QDE /	> 0.7
Energy range:	3 – 13 keV
Average count rate density:	~ 10^6 count/cm^2.s
Peak count rate density:	~ 10^7 count/cm^2.s
Read out time	~ 10 ms

Simulation results for ITER ITB

C Ingesson et al HTPD 2004

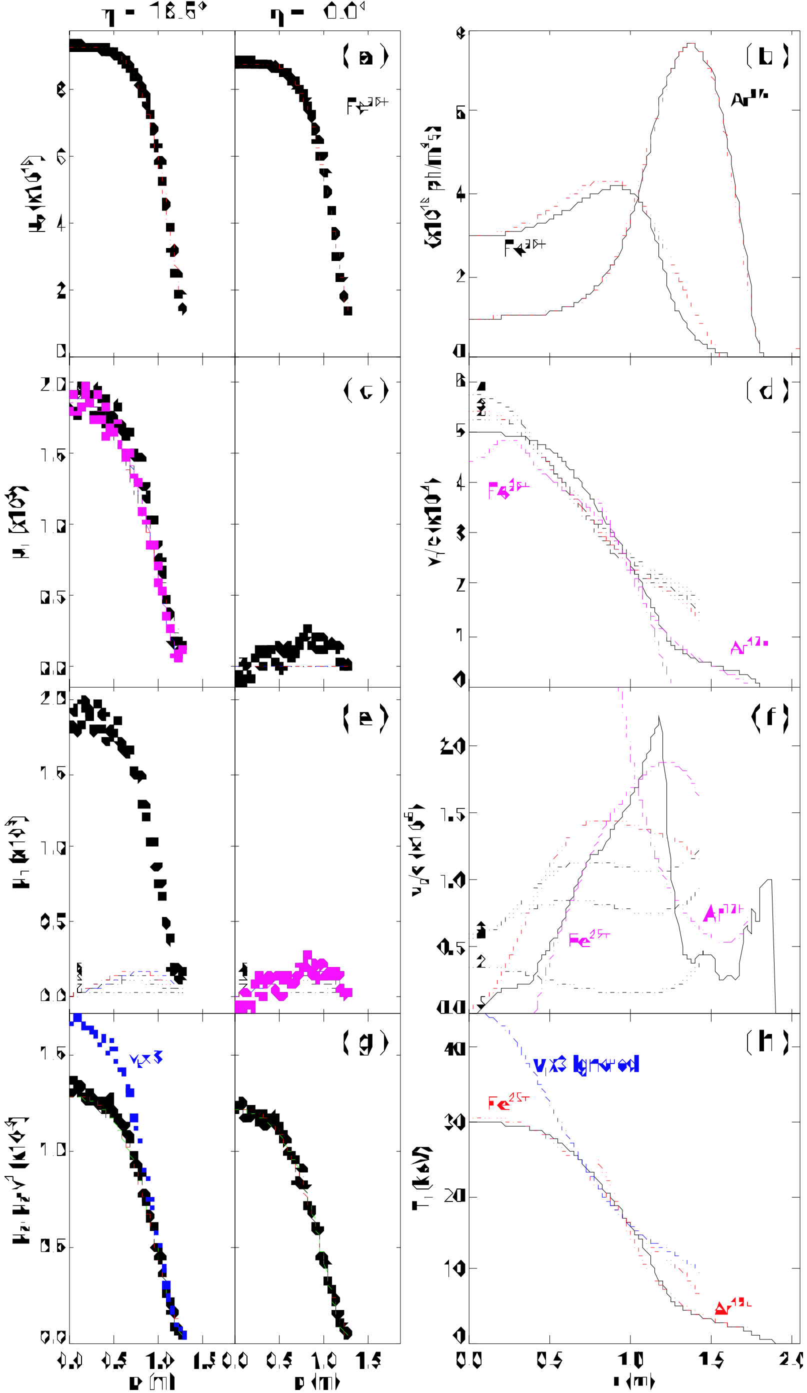

- Fe concentration of 10^{-5}
- H-like line at 1.784 Å
- Integration time of 0.3 s

Two views of the top half of the plasma were assumed measuring at toroidal angles h = 0° and 18.5°.

Left-hand column: moments calculated from the simulated measurements (solid circles) and backcalculated moments from the reconstruction (curves).

Right-hand column: input profiles of the simulation (solid curves) and reconstructed profiles (dotted lines).

Rows, from top to bottom:
emissivity, toroidal rotation, poloidal rotation and T_i.

MEDIPIX2 Hybrid Pixel Detector

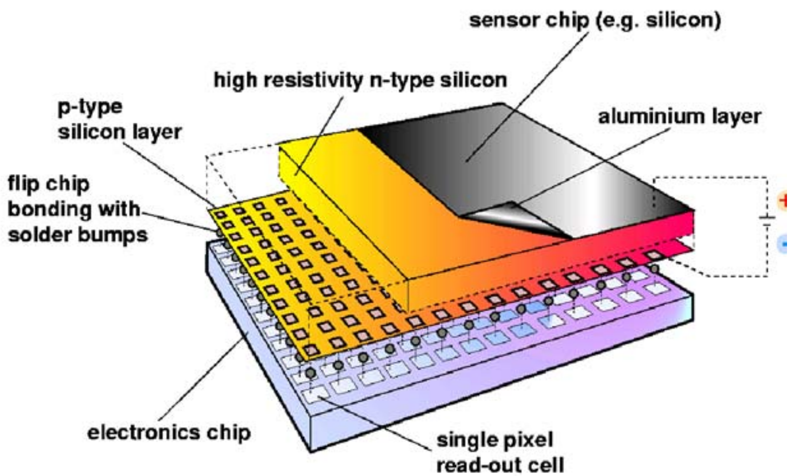

Detector and electronics readout are optimized separately

Medipix2 Cell Schematic

Charge sensitive preamplifier with individual leakage current compensation
2 discriminators with globally adjustable threshold
3-bit local fine tuning of the threshold per discriminator
1 test and1 mask bit
External shutter activates the counter
13-bit pseudo-random counter
1 Overflow bit

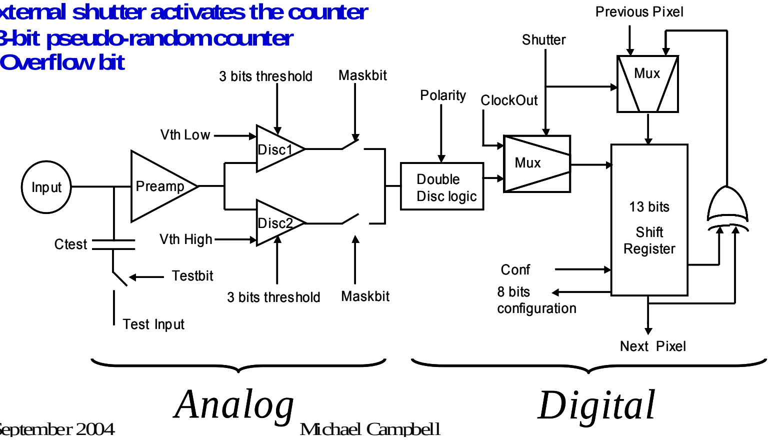

Medipix2 Cell Layout

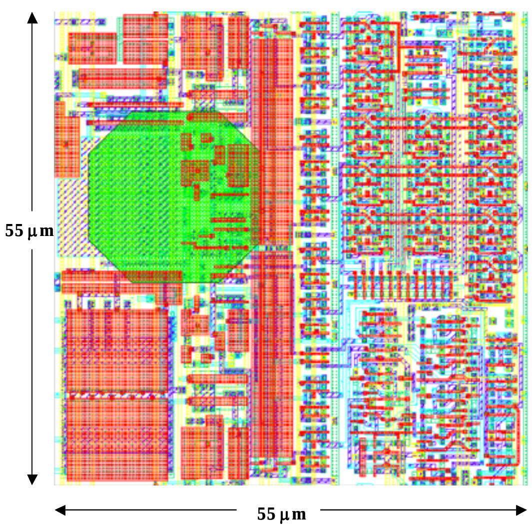

Medipix2 Chip Architecture

256 x 256 pixels
3ms readout time

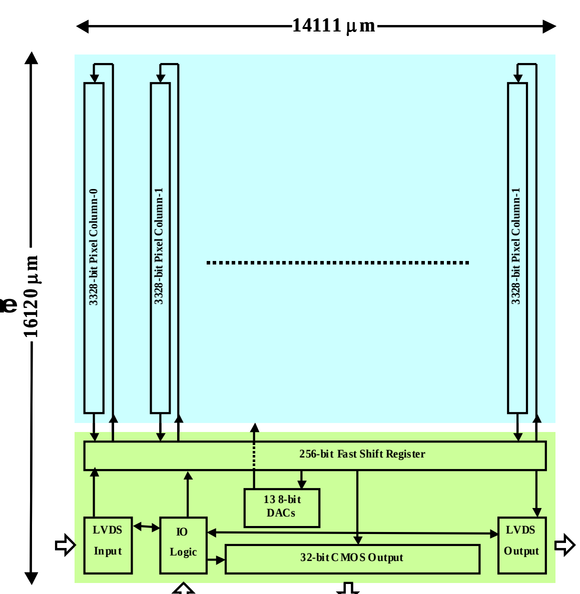

The revolution in x-ray/particle detectors

CERN Medipix II active pixel detector

Applications:

- X-ray imaging PHA
- Imaging X-ray crystal spectrometer
- Counting heavy ion beam probe
- Compact (imaging?) NPA

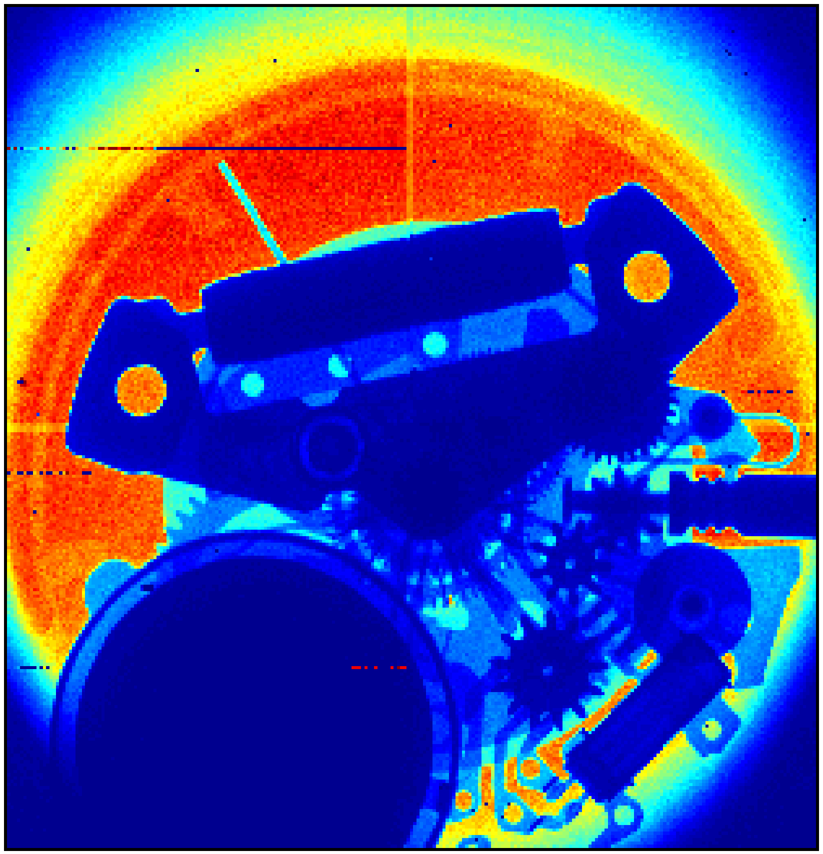

Medipix II in 2 x 2 array

Photon-counting ~ 5% energy-window at ~20 keV

Medipix II with USB interface

The JET D-T compatible soft x-ray cameras

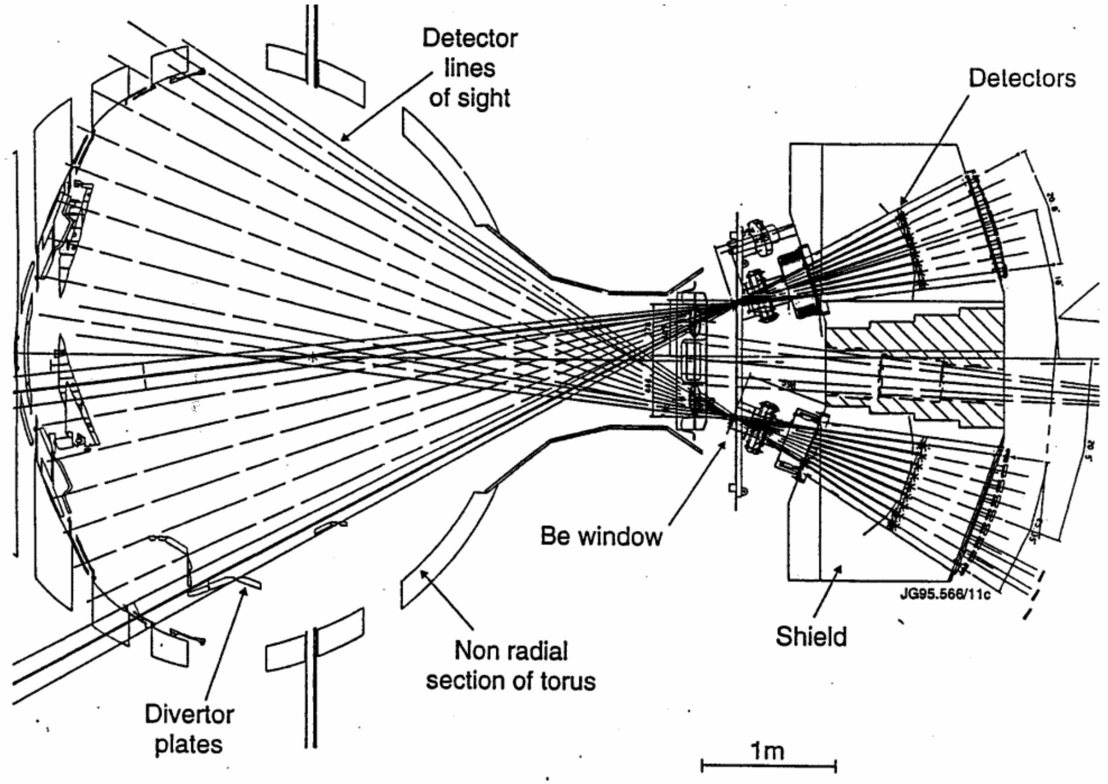

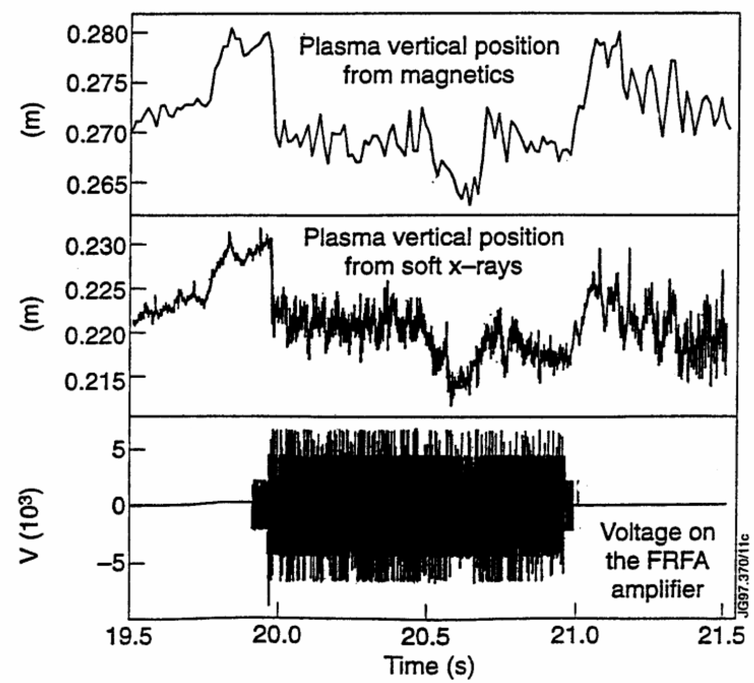

Demonstration of plasma vertical stabilisation from 20 - 21 s, using the soft x-ray control signal.

Update of x-ray camera on Eq 09

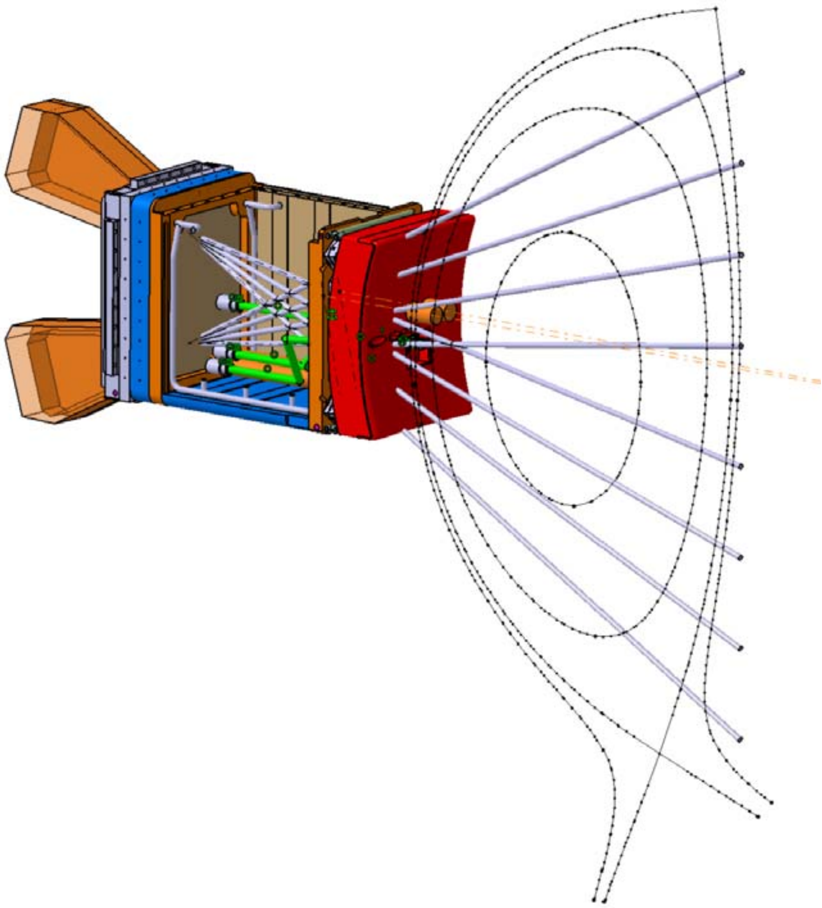

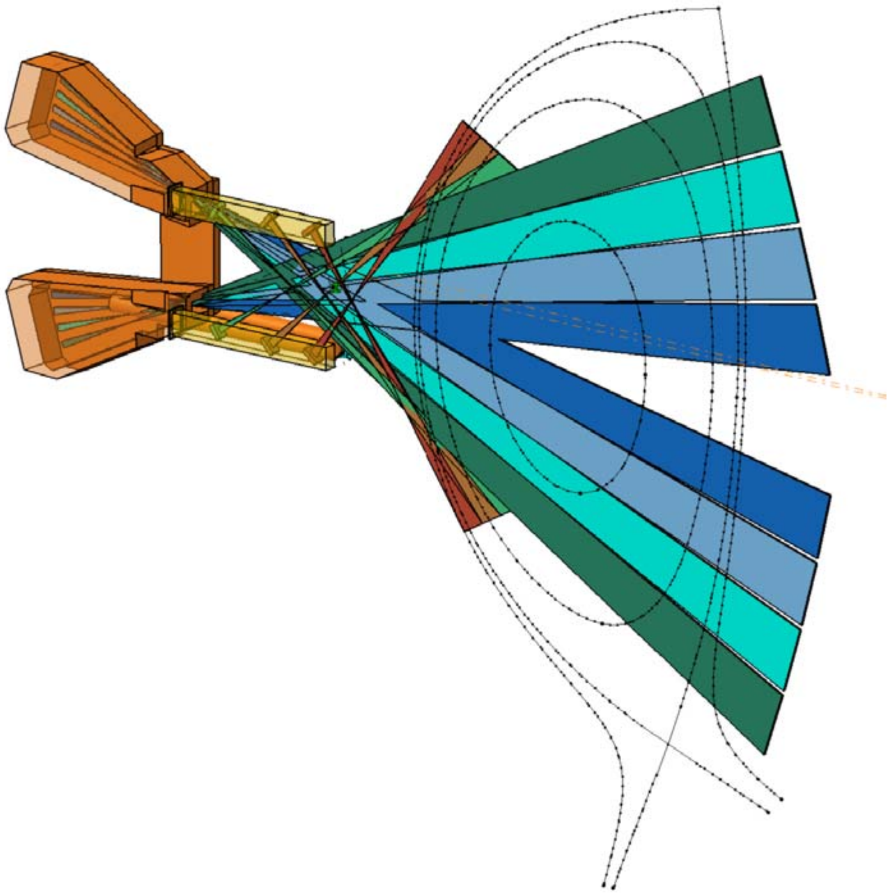

Reference design

Based on JET D-T x-ray camera “KJ5”

Discrete chords

Continuous poloidal resolution

Outer plasma viewed by in-port detectors in removeable cassettes

SANCO/ADAS modelled x-ray emission for ITER Te, Ne profiles

Martin O'Mullane, Strathclyde University & EFDA/JET

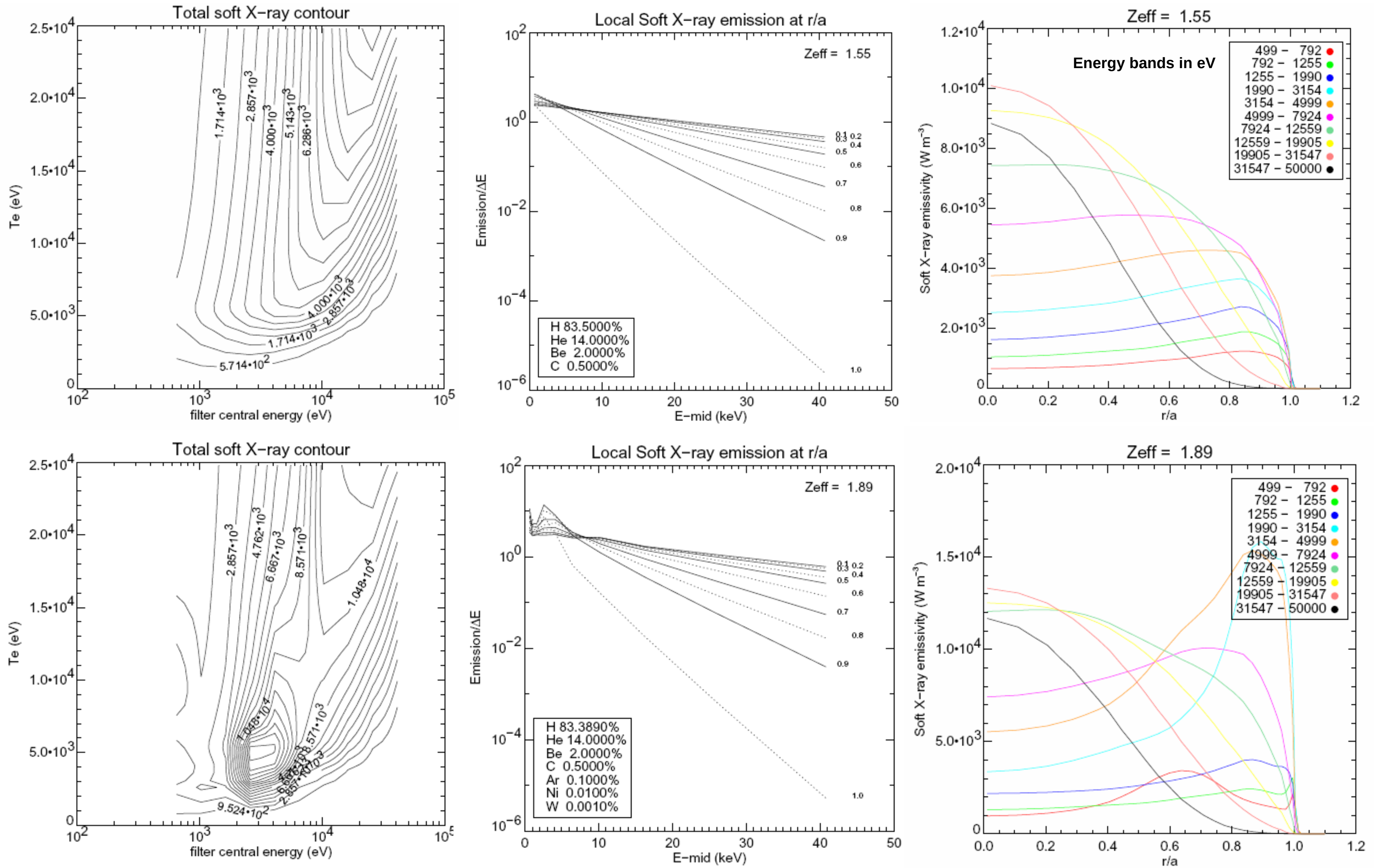

Estimates of x-ray and neutron emission

Approximate analytical expression for x-ray continuum

(ph/cm^3.s.eV)

$$\varepsilon ph_{ff}(E,r) := \frac{10^{-7}}{h \cdot E} \cdot 6.4 \cdot 10^{-40} \cdot \zeta \cdot \frac{Ne(r)^2}{Te(r)^{0.5}} \cdot Z_{eff} \cdot g_{ff} \cdot e^{\frac{-E}{Te(r)}}$$

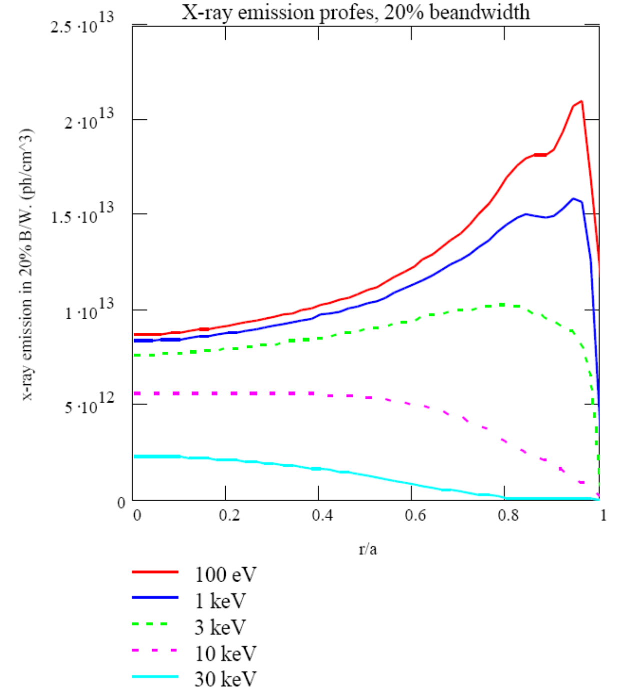

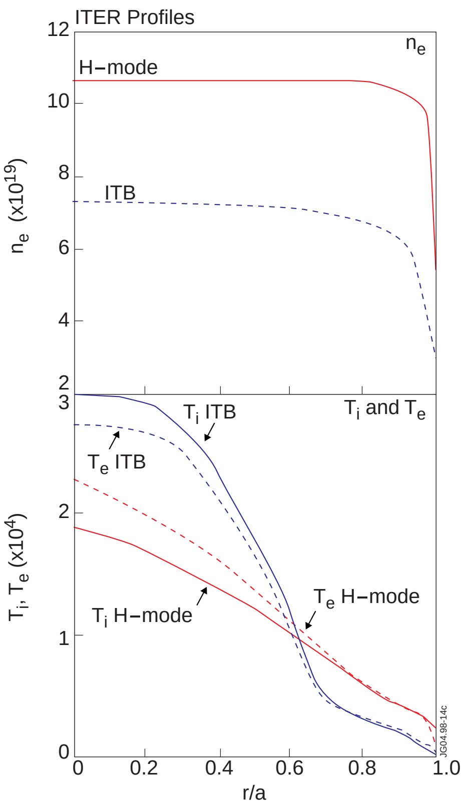

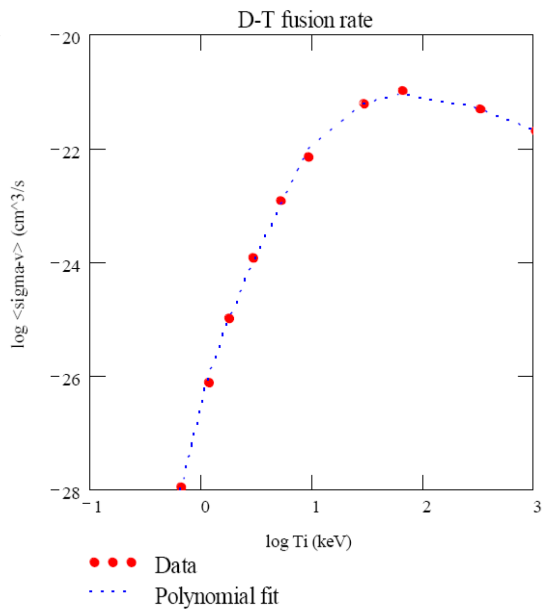

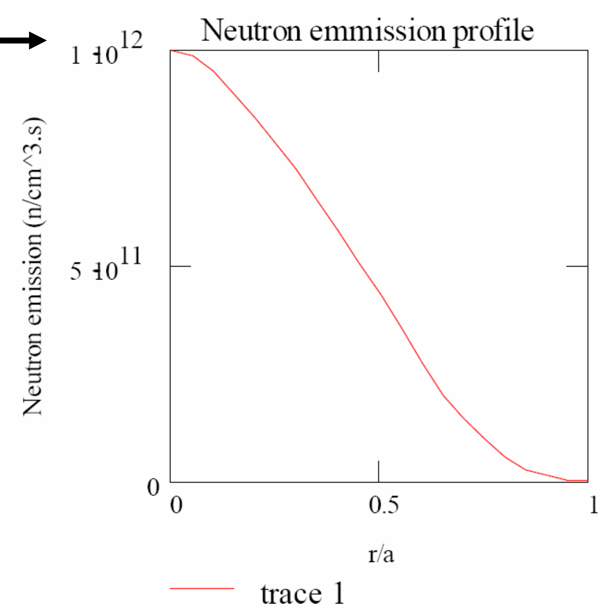

Outline parameters of ex-vessel x-ray camera module

- Narrow angle of view to maximize neutron shielding
- Window can be substantial eg 1-5 mm Be or **1-2 mm diamond**
- Detector: Fast, radiation-hard, photon-counting, energy-resolving position-sensitive detector
    - eg CERN-Medipix, PSI-Pilatus, ENEA-Pacella

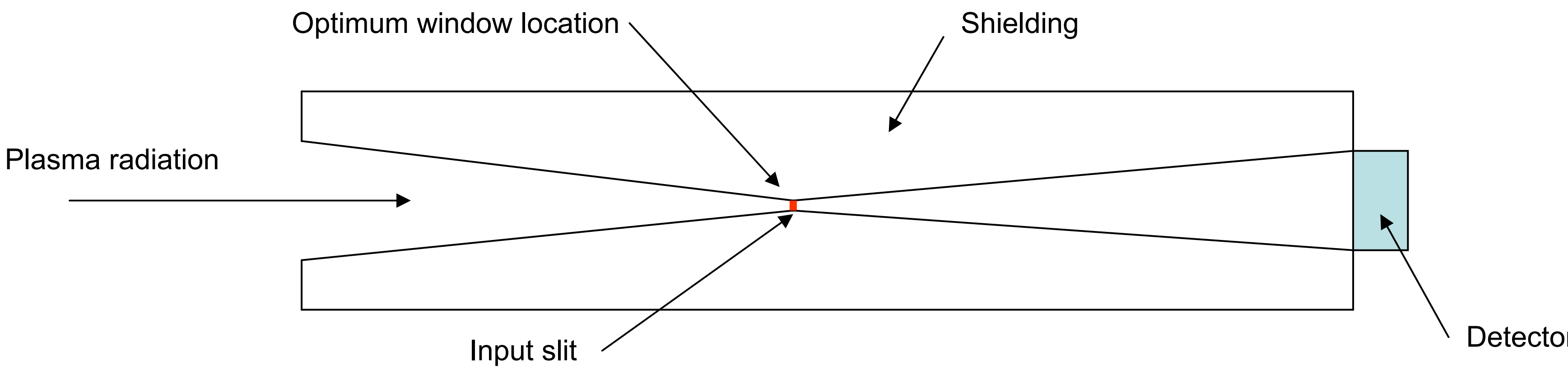

Outline dimensions		Detector performance	
- Entrance slit to detector:	~ 1 m	- 1d spatial resolution:	<~ 250 um
- Entrance slit to plasma:	~ 5 m	- Energy range:	1 – 100 keV
- Slit width x height:	1 x 5 mm^2	- Multi-channel energy resolution:	5 -15%
- Angle of view:	5 deg.	- Peak count-rate:	1.5 . 10^9 /cm^2.s
- Poloidal resolution for 1mm slit:	5 mm	- Max direct neutron flux:	6 . 10^6 /cm^2.s
- Blanket slot width:	< ~20 mm	- Time for n-fluence of 10^14 /cm^2:	~ 10^7 s

Ex-vessel x-ray camera in Eq 09

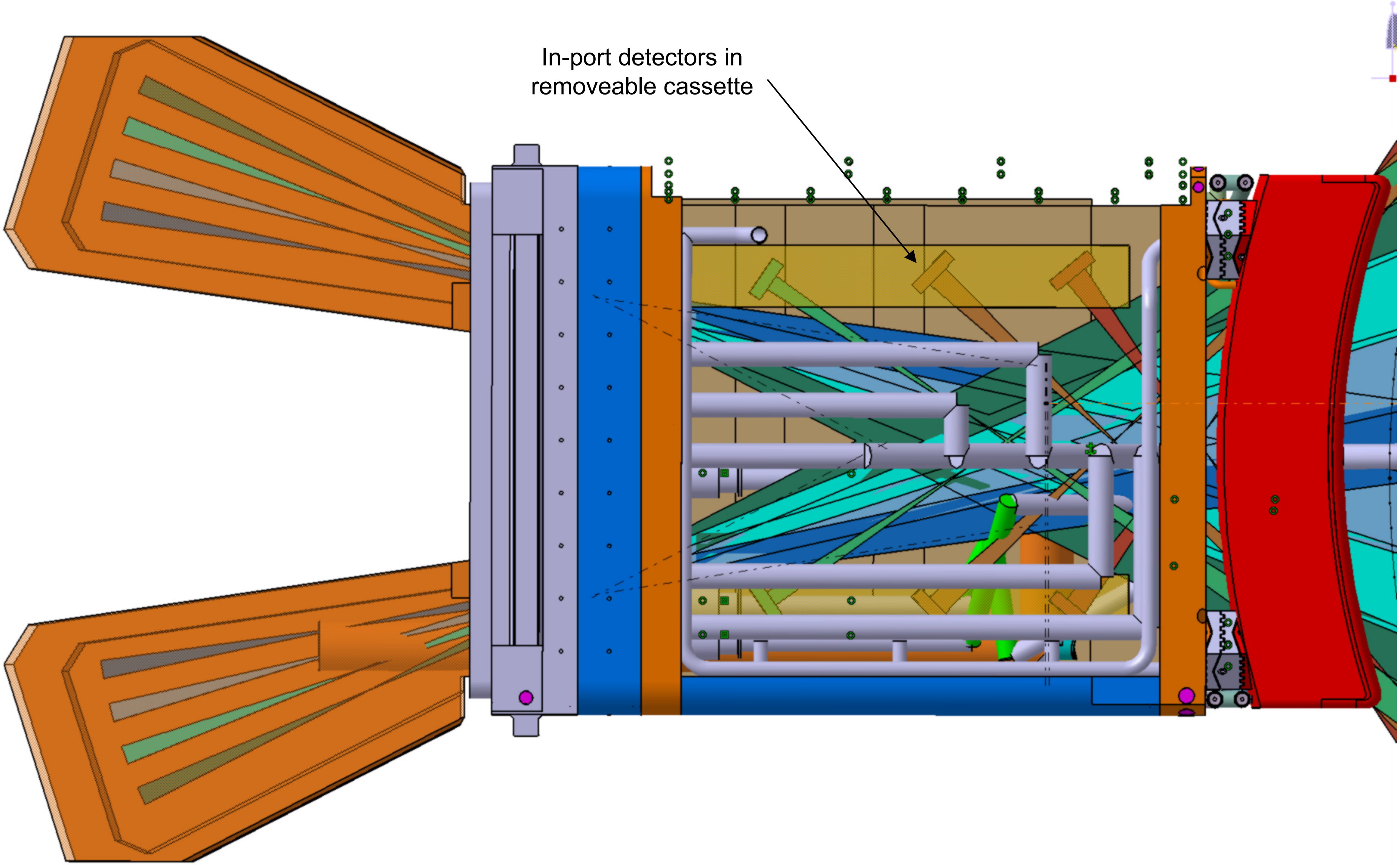

Signals, and emission reconstruction

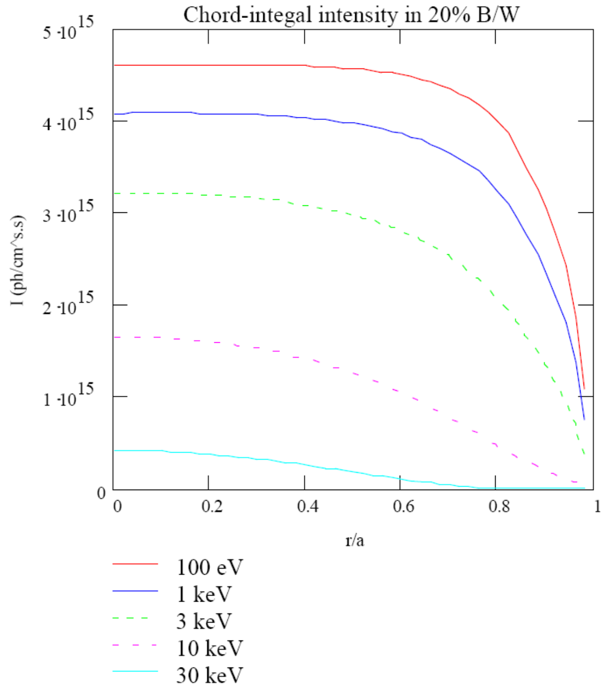

+ Instrument geometry
+ 1 mm Be window
+ Detector QDE
(x-ray 0.5, and neutron 1.0)
+ Poisson counting noise
+ Neutron background
(only direct so far)

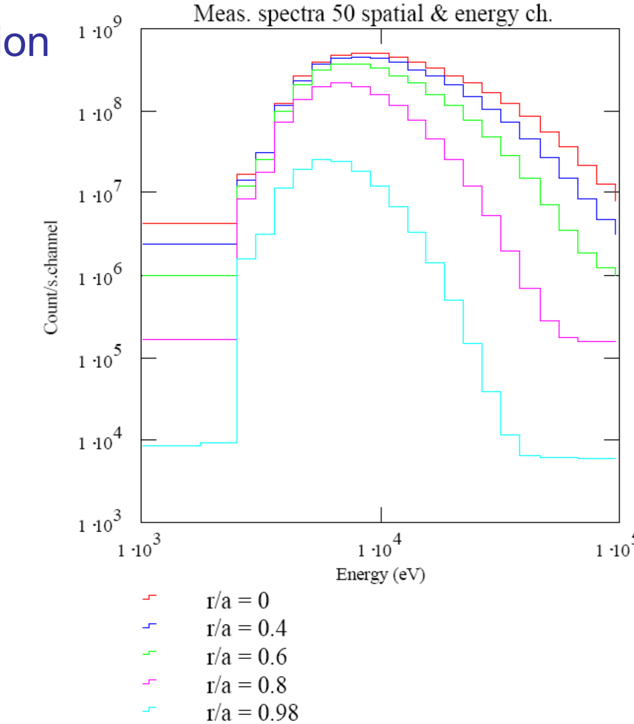

Analytic Abel inversion

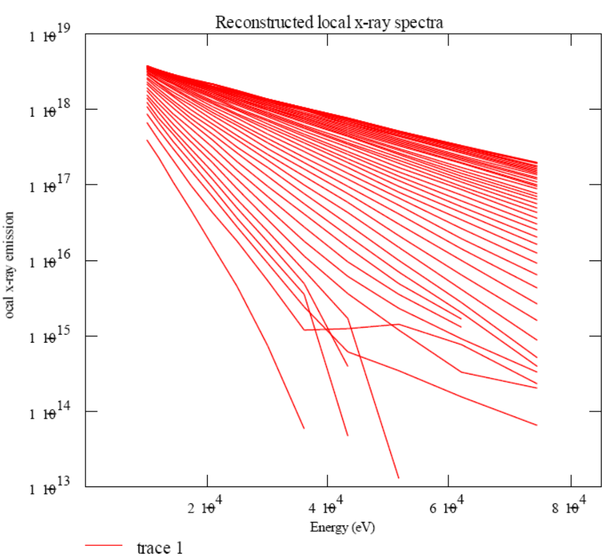

Fit 1/e gradient for local Te at each chord

Artefact due to fixed energy range for fit at each chord. Can be improved

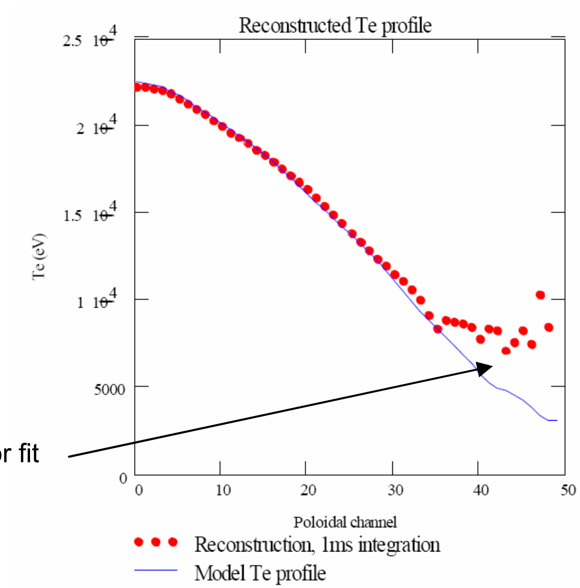

ADAS/SANCO modelled ITER broadband x-ray spectra

Line and continuum in 5% energy bands, radially resolved

< 10 keV: mainly impurity information

> 10 keV: mainly Te information

Modern detectors will be able measure this…

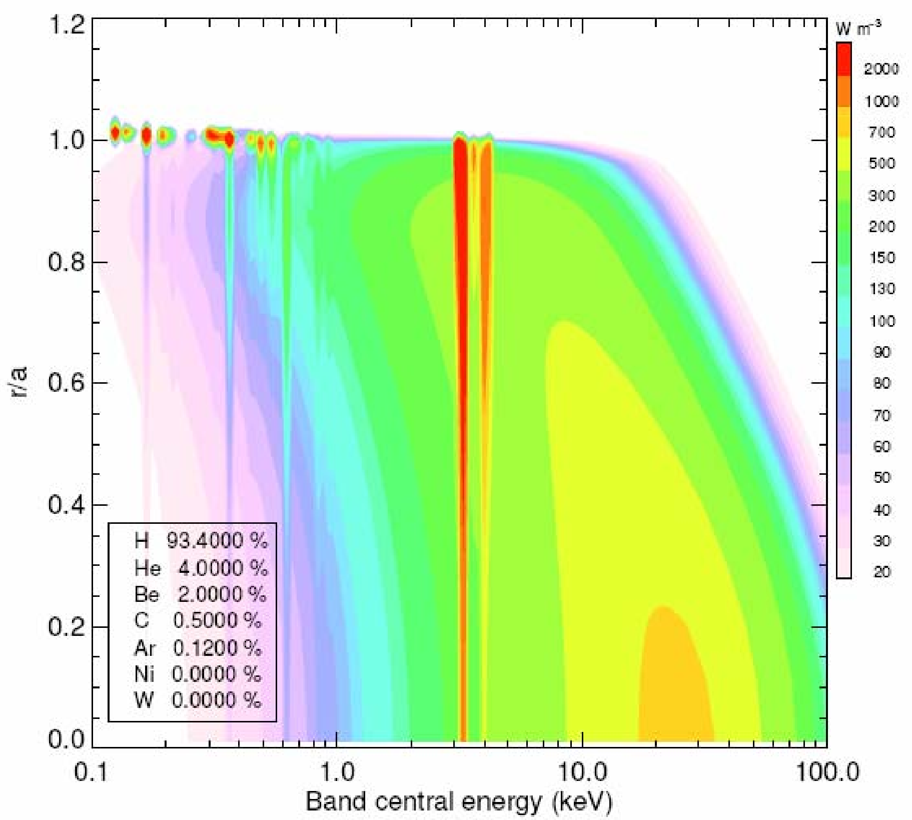

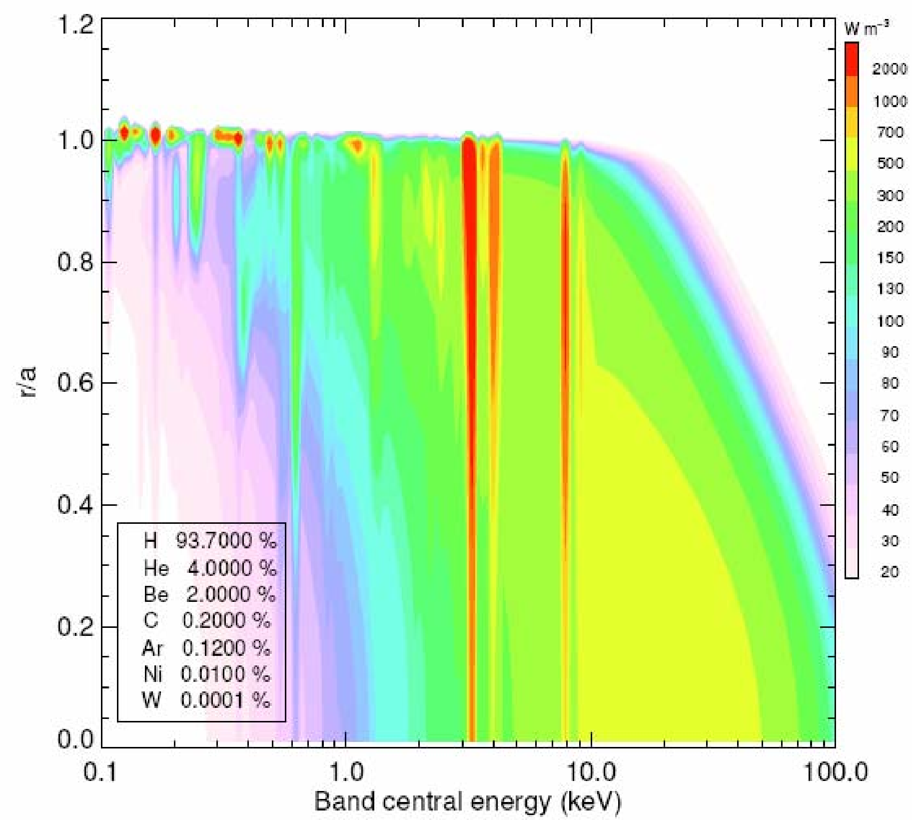

Summary

- ADAS contributes to ITER on several levels:
    - Clarification of VUV measurement requirements
    - Input to x-ray spectrometer design
    - Prospects for a spectroscopic x-ray camera
    - Impurity radiated power (M O'Mullane, this meeting)
    - Beam-aided spectroscopy (M Von Hellerman, this meeting)
- Future:
    - All impurity radiated power components for power balance
        -Start-up, operating scenarios etc.
    - Prediction of Tungsten spectrum
        - Visible: contamination etc
        - VUV: diagnostic potential, especially divertor
        - X-ray: diagnostic potential for Ti profiles

SLHC and tracking

	LHC (2007)	SLHC (2015)
Proton Energy:	7 TeV	12.5 TeV
Collision rate:	40 MHz	80 MHz
Peak luminosity:	10^{34} cm^{-2}×s^{-1}	10^{35} cm^{-2}×s^{-1}
Int. luminosity:	500 fb^{-1}	2500 fb^{-1}

~ 100 pile-up events per bunch crossing for 12.5 ns bunch spacing compared to ~20 at 10^{34} cm^{-2} s^{-1} and 25 ns

- If same granularity and integration time as now, the tracker occupancy and radiation dose increases by a factor of 10 ⇒ implication for radiation damage and physics

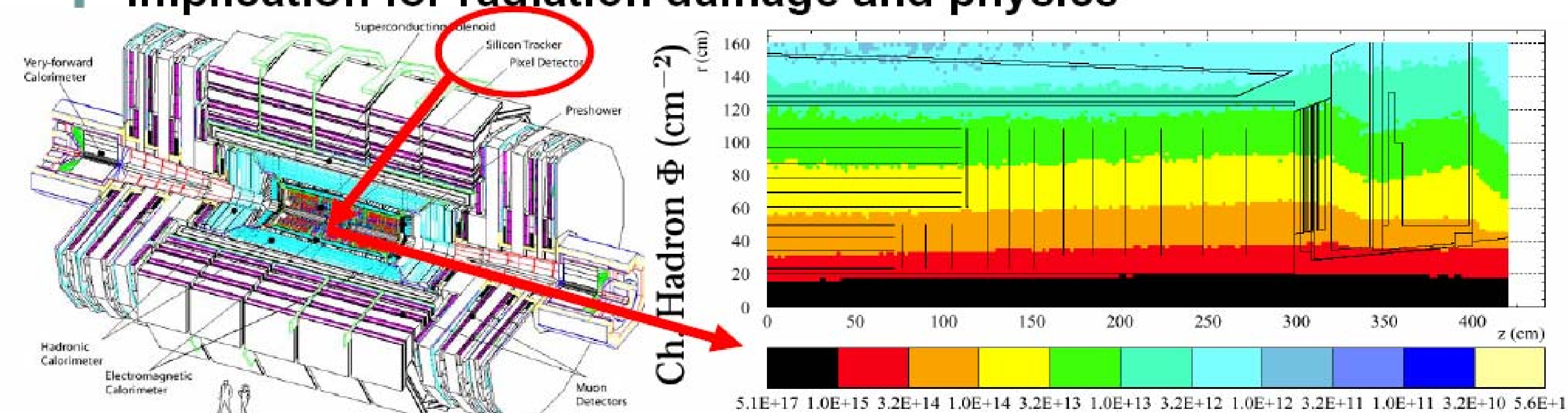

M. Hutinen: "Radiation issues for Super-LHC", SLHC Electronics Workshop, 26/2/04, CERN

Daniela Bortoletto Vertex 2005 Nikko Japan **6**

SLHC and tracking

- $dn^{cha}/d\eta$/crossing ≈600 and ≈3000 tracks in tracker ⇒more granularity if we aim at same performance we expect from the LHC trackers

H→ZZ→eeμμ m(higgs)=300 GeV all tracks with p_T<1 GeV removed

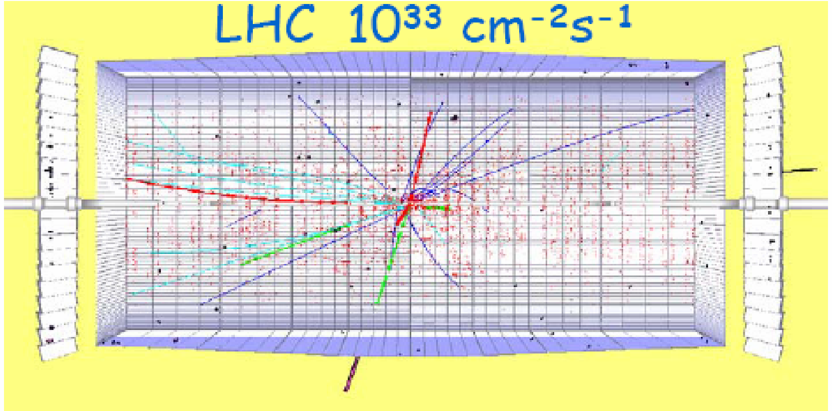

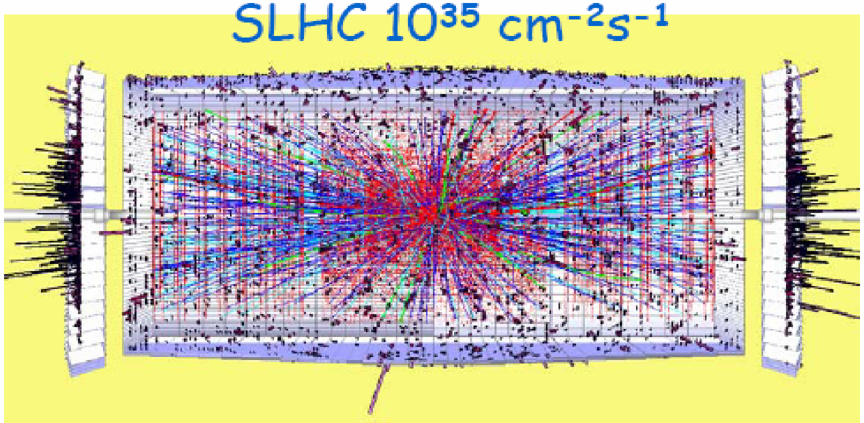

- **Integrated Luminosity** (radiation damage) dictates the detector **technology**
- **Instantaneous rate** (particle flux) dictates the detector **granularity**

R (cm)	Φ (p/cm^2)	Technology
>50	10^{14}	Present p-in-n (or n-in-p)
20-50	10^{15}	Present n-in-n (or n-in-p)
<20	10^{16}	RD needed